New Zealand Water Accounts Update 2020

Prepared for Stats NZ Tatauranga Aotearoa

May 2021

Climate, Freshwater & Ocean Science

Citation
Griffiths, J, Zammit, C, Wilkins, M, Henderson, R, Singh, S, Lorrey, A, Shankar, U, Vargo, L, Anderson, B, & Purdie, H (2021). *New Zealand water accounts: Update 2020*. NIWA report prepared for Stats NZ Tatauranga Aotearoa. Retrieved from www.stats.govt.nz.

ISBN 978-1-99-003252-3

Published in May 2021 by
Stats NZ Tatauranga Aotearoa
Wellington, New Zealand

Contact
Stats NZ Information Centre: info@stats.govt.nz
Phone toll-free 0508 525 525
Phone international +64 4 931 4600

www.stats.govt.nz

Prepared by:

James Griffiths
Christian Zammit
Matt Wilkins
Roddy Henderson
Shailesh Singh
Andrew Lorrey
Ude Shankar
Lauren Vargo
Brian Anderson
Heather Purdie

For any information regarding this report please contact:

Christian Zammit
Hydrologist
Hydrological Processes
+64-3-343 7879
christian.zammit@niwa.co.nz

National Institute of Water & Atmospheric Research Ltd
PO Box 8602
Riccarton
Christchurch 8011

Phone +64 3 348 8987

NIWA CLIENT REPORT No: 2020325CH
Report date: May 2021
NIWA Project: SNZ20502

Revision	Description	Date
Version 1.0	Draft Report	20 November 2020
Version 1.1	Final Report	22 March 2021
Version 1.2	Revised Final Report	14 May 2021

Quality Assurance Statement		
	Reviewed by:	Scott Larned
	Formatting checked by:	Rachel Wright
	Approved for release by:	Helen Rouse

Contents

Tables

Figures

Executive summary

Stats NZ Tatauranga Aotearoa (StatsNZ) requested water stock accounts for the period 1995 to June 2020 inclusive. This technical report summarises the data held on national and regional water flows (precipitation, evapotranspiration and rivers) and storage (ice and snow, soil moisture, lakes and hydro-electric generation water use).

The data have been summarised by annual mean (defined by the hydrological year: 1 July to 30 June) and seasonal means (yearly quarters: July to September; October to December; January to March; and April to June). The data summaries are organised by the 16 regions of New Zealand.

Analysis of the data shows that precipitation, river flows to the sea, and evapotranspiration are major components of the water cycle. It is also shown that abstraction/discharge by hydro-generation is a substantial non-consumptive use of water. Some comparison with the previous reporting (Henderson et al. 2011) has been made and it was noted that at a national scale, the current reporting period was one of reduced precipitation (and thus surface water flows). However, this pattern varies depending on the region.

It is noted that whilst there is uncertainty in both observed data and model output, validation checks on the dominant modelled data used (precipitation and river flows) provide confidence in the presented results.

The datasets illustrated in this report, and associated R code used to prepare that data, also form part of the deliverables of this project.

1 Introduction

Statistics New Zealand Tatauranga Aotearoa (StatsNZ) has previously produced four iterations of the national Water Physical Stock Accounts including 1995–2001, 1995–2005, 1995-2010 and 1995-2014 (see Collins et al. 2015). For each iteration, NIWA supplied StatsNZ with a technical report and summary data on surface water flows and storage (including glaciers, lakes and hydro-electric generation water use). This report represents a water physical stock account for the period 1995 to June 2020 inclusive. The report includes data summaries and technical descriptions of methods used in their preparation. Corresponding datasets and computing code are also provided as deliverables of this project. Analysed datasets can be described in three categories:

- **Inflows (into a region):** precipitation, inflow from other regions;
- **Outflows (from a region):** evapotranspiration, outflow to other regions, outflows to sea;
- **Changes in Storage:** soil moisture, lakes and reservoirs, snow, and ice.

Data on water abstraction for hydroelectricity generation, and water discharge from hydroelectricity generation are also provided. All data are provided at the regional scale and summarised at a national scale. All variables are expressed in units of cubic metres. It should be noted that changes in water use have not been calculated.

The methods used in preparation of these accounts are unchanged from previous accounts except for: a) the inclusion of large surface water bodies within the river network used by the New Zealand Water Model (NZWaM[1]) (i.e., lakes, hydroelectric reservoirs and wetlands with surface areas greater than 1 ha); b) use of a new formulation of evapotranspiration processes (improving previous evaporation estimates); and c) calculation of the annual water amount stored as ice (change in methodology). For uniformity across New Zealand, such water bodies are modelled as naturally draining features. Climate, land cover and river network datasets used to generate the accounts have been updated to reflect changes in national scale information available for hydrological modelling across New Zealand (for description of data sources see Yang et al. (2017)).

This report is structured to provide:

- a description of each component of the water accounts and its source data
- national and regional summaries of each component of the water accounts and the relative changes since the previous account report
- descriptions of the intra-annual variability
- a description of the sources of uncertainty, and
- validation of hydrological and climatological observation data.

All annual data are summarised with respect to the hydrological year (1 July to 30 June). Seasonal data are organised in yearly quarters: July to September; October to December; January to March; and April to June. The naming convention used describes the hydrological year by the year in which the data set ends (e.g., 1 July 1994 to 30 June 1995 is described as the year 1995).

[1] NZWaM is the national modelling framework that now includes the TopNet surface water model that was used in previous water accounts (albeit with some improvements in representation of evapotranspiration processes).

2 Water accounts 2020

The water accounts in this report consist of eleven variables for 16 regions of New Zealand (see Appendix A), for the period 1995 to 2020. Definitions of the components of the water accounts and the data sources used in their derivation are listed in Table 2-1. In addition to this report, regional scale processed data are provided to StatsNZ, with a repository for the R codes used in compilation of the data at: https://git.niwa.co.nz/nzwam/topnet-reg-summary (see also Appendix B).

Table 2-1: Water account components and the source data from which they have been derived. All components are expressed as mean annual and mean seasonal values in this report.

Component name	Description	Source
Precipitation	The total volume of rain/hail/snow/sleet.	New Zealand Water Model (NZWaM) rainfall input, derived from the Virtual Climate Station Network (VCSN).
Evapotranspiration	The total volume of water lost by evapotranspiration (actual rather than potential).	Calculated by NZWaM, based on temperature dependent potential evapotranspiration, water availability (calculated soil moisture) and vegetation characteristics.
Outflow to sea	The total volume of water that flows to the sea (does not consider prior water abstraction).	Output of surface water component of NZWaM.
Outflow to other regions	The total quantity of surface water that leaves a region and flows to another region.	NZWaM flow data output with GIS analysis of river networks and administrative regional boundaries.
Inflows from other regions	The volume of water that enters a region from outside that region (includes non-riverine water transfers).	NZWaM flow data output with GIS analysis of river networks and administrative regional boundaries.
Hydro-generation abstraction	The total volume of water abstracted from surface water for electricity production by hydro-generation companies.	Derived from measured power station machine flows (does not include spill flows).
Discharge by Hydrogeneration	The total of water discharged by hydro-generation companies.	Is equivalent amount to water abstracted for hydro-generation.
Change in Lakes	The change in volumes of lakes and reservoirs.	Derived from recorded hydro-lake level data.
Change in Soil Moisture	The change in volume of water stored in soil.	Derived from NZWaM output.
Change in Snow	The change in quantity of water stored as frozen water (permanent and seasonal snow/ice).	Derived from NZWaM output.
Change in ice	The change in quantity of water stored in ice.	Derived from end-of-summer snowline survey (EOSS), and observation of pro-glacial lake development and down-wasting.

2.1 National trends

Figure 2-1 represents the coarsest resolution of the analysed accounts data and illustrates the mean annual water flux for the whole of New Zealand over the period 1995-2020 (current accounting period) compared to 1995-2014 (previous accounting period). It should be noted that the results shown for the previous accounting period will differ slightly from results shown for the same period in the previous report (Collins et al. 2015) due to changes in the way that evapotranspiration has been calculated (as described above). Also shown are the mean values for 2015-2020 which reflect an increase in climate variability and increased frequency of extreme weather events in that period (e.g., the 2017 marine heatwave). The period 2015-2020 is characterised by i) lower mean precipitation (and thus total outflow to the sea) in the last five-year period compared to the mean of either of the other periods; and ii) an increase in temperature in the 2015-2020 period (not included as part of the water account reporting variable). Figure 2-2 illustrates the corresponding mean annual change in water storage over the same periods. In response to reduced mean annual rainfall and increased temperature in the last five years, there is a corresponding reduction in mean annual lake and soil moisture storage across the same periods.

Figure 2-3 and Figure 2-4 illustrate the change in mean annual precipitation (m^3) from 1995 to 2020 for the North Island and South Island respectively. Again, it can be seen that the last five years have been characterised by decreasing annual rainfall volume (particularly 2016-2018 in the North Island). This trend is less pronounced in the South Island (and reversed in the West Coast and Southland regions) indicating potential persistent shift in historical weather patterns that could be associated with detection of climate change signal on cryospheric processes.

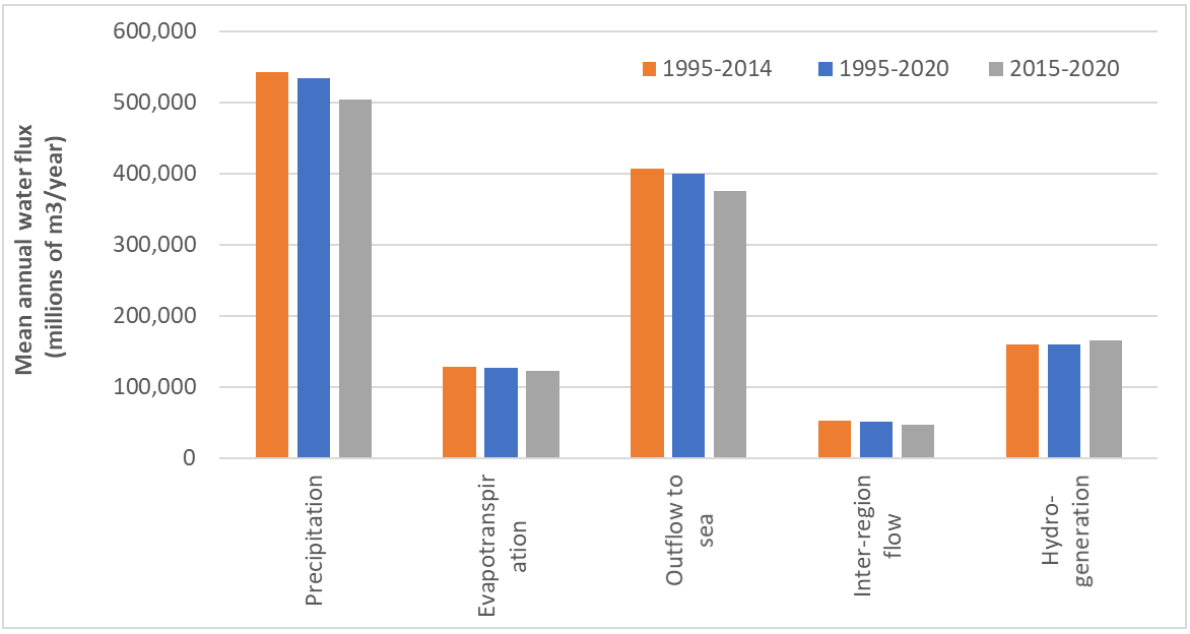

Figure 2-1: Comparison of mean annual water flux for the periods 1995-2014, 1995-2020 and 2015-2020.

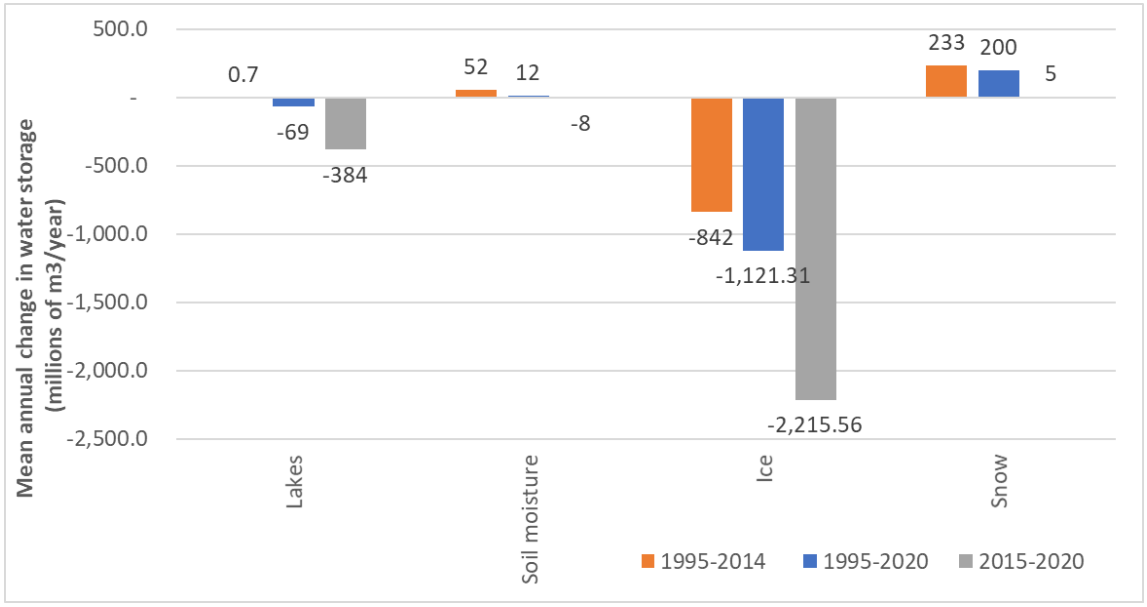

Figure 2-2: Comparison of mean annual change in water storage for the periods 1995-2014 and 2015-2020. (note change in ice volume is to end of 2019 only).

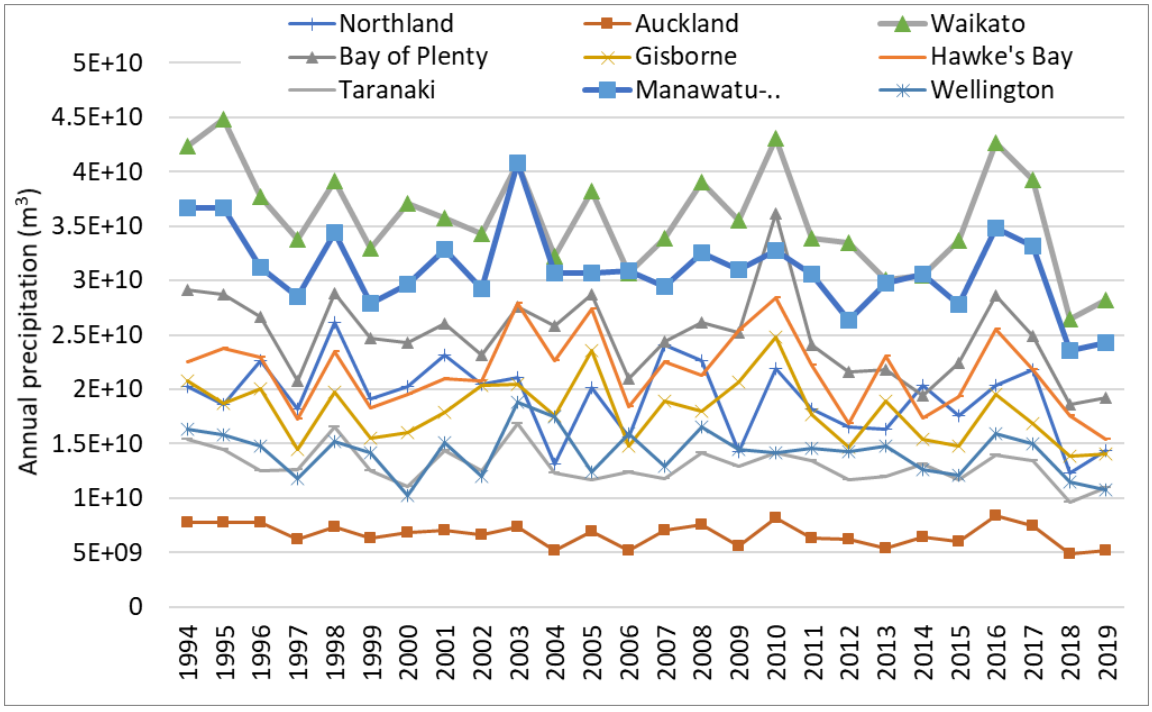

Figure 2-3: Mean annual precipitation volume (m3) in north island regions from 1995 to 2020.

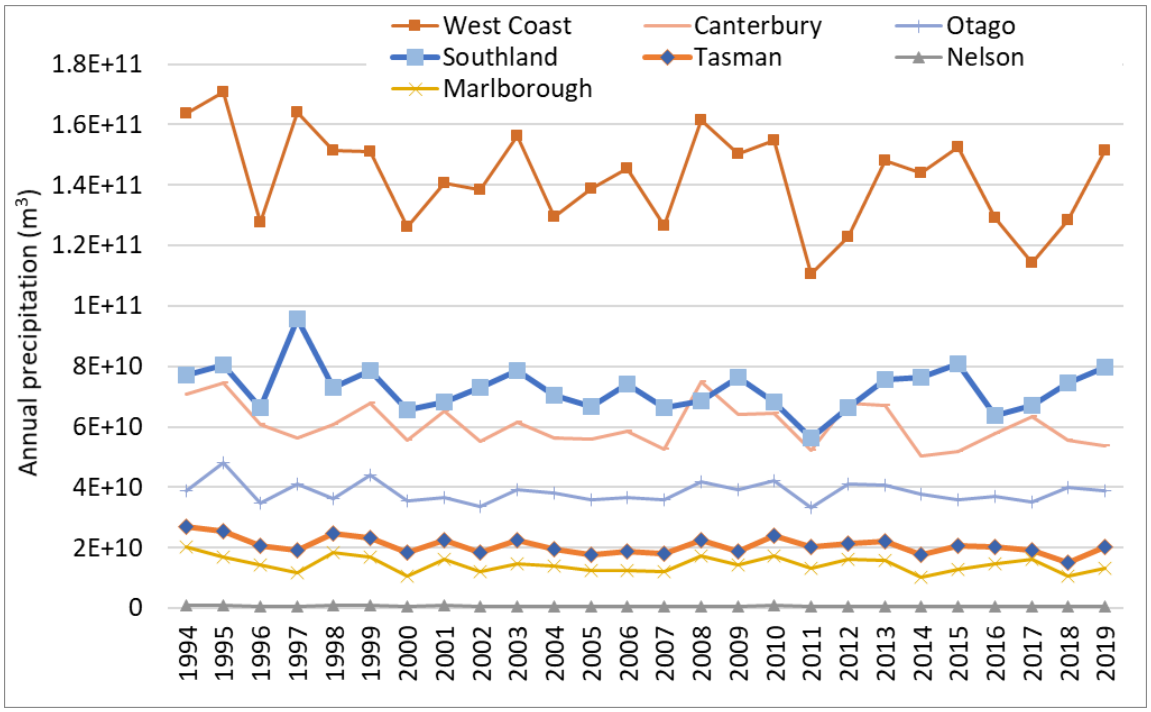

Figure 2-4: Mean annual precipitation volume (m3) in south island regions from 1995 to 2020.

2.2 Differences between 2020 and 2015 water accounts

There are several differences between the 2015 and 2020 water accounts. These differences are due to a number of changes in accounting methodology since 2015 including: i) changes to hydrological process conceptualisation within the surface water model; ii) changes to the reporting frequency of some variables; iii) changes in the methodology used to calculate specific components of the water account; and iv) changes in datasets used to calculate the water account. These differences are described in more detail below.

2.2.1 Difference in process conceptualisation

The surface water model used in compilation of the water accounts was relatively consistent between the 2015 and 2020 accounts. The only change has been in the conceptualisation of evapotranspiration processes. For the 2020 water account a "Feddes" conceptualisation of the evapotranspiration (Feddes et al. 1978) has been implemented. This addresses a tendency to underestimate evapotranspiration in the previous water accounts. As a result, it is expected that mean evapotranspiration, discharge to sea, change in soil moisture, and inter-regional transfers, will differ from the previous version of the water accounts (increased evapotranspiration and decreased surface water availability).

It should also be noted that a new temperature dataset is used in calculation of snowfall. A seasonal lapse rate is now used instead of a fixed lapse rates, as a result seasonal or annual snow accounting is not comparable with previous versions of the water accounts.

2.2.2 Difference in reporting frequency

The 2020 account reports the component water accounts at annual and seasonal time scale (see Appendix B for the definition of the seasons reported) as opposed to just annual time scale as per the 2015 accounts. As a result, some of the components of the water account (such as Hydropower flows

and Lake storage) were not completed or were only partially completed at the time of the analysis (see 2.2.4.2 for more information).

2.2.3 Difference in methodology

Two methodological changes were made as part of the 2020 surface water accounts.

2.2.3.1 Ice storage calculation

In the 2020 account, the ice modelling team used a new methodology to calculate ice storage and ice storage change. This methodology overcomes methodological issues associated with the method used in previous accounts and it takes into account the latest technological developments that have occurred between 2015 and 2020 (see Appendix C for more information). As a result, there is less uncertainty associated with the 2020 ice storage calculation compared to the the 2015 ice storage calculation.

2.2.3.2 Inter-regional flow transfer calculation

Due to updates to the digital river network, a new method was used to identify surface water inter-regional flow transfers. To do this, for all sub-catchments in New Zealand, two points were defined, a centroid and an outlet. The centroid is defined from the sub-catchment boundary and the outlet is defined as the most downstream point of the sub-catchment. Inter-regional flow is then identified where the centroid and outlet of any sub-catchment lie in different regions. For example, inter-regional flow occurs where the bulk of a sub-catchment lies in one region and the outlet of the catchment lies in another. It should be noted that the existence of inter-regional flow may lead to higher total regional outflow (to oceans) than inflows (precipitation), (e.g. Otago).

A visual inspection of identified inter-regional flow transfers was performed to verify the above algorithm. As a result, the predicted inter-regional discharge estimation in this report is larger than that of previous water accounts.

2.2.4 Difference in datasets

2.2.4.1 Hydrological model

The surface water accounts rely on five spatial datasets provided to NZWaM: i) national scale topographic information provided in a DEM; ii) a digital river network; iii) land cover information; iv) a soil map characterising shallow soil information across New Zealand; and v) geological information. For this version of the account, an updated version of the digital river network (version 2.4), was used instead of version 1.2 as per 2015 water accounts. An updated version of the Land Cover Database (version 4) was also used to generate land cover information across New Zealand. These two changes are not expected to yield significant differences in water accounting at regional scale but could lead to small amounts of local-scale water being routed to different locations in the digital river network.

2.2.4.2 Lake dataset

Major lake differences between the 2015 and 2020 water accounts are summarised below (reported per administrative region):

1. Auckland: 11 lakes (many reservoirs) instead of just two in the 2015 report.

2. Canterbury: some differences in pre-2000 data, possibly because of editing by data owners.

3. Tasman: 15 more years data for the only significant lake, compared to the 2015 report.

4. Wellington: the 2015 account did not use data previously used for a coastal lagoon and two small water supply reservoirs (as they are only used to store clean water while rivers are in flood). No data for a reservoir that had only four years of data in 2015.

5. West Coast: some differences between the 2015 and 2020 accounts in the availability of pre-2000 data.

Table 2-1 presents a summary of the level of completeness of the information used in the lake component of the 2020 water accounts.

Table 2-2: Summary of the 2020 lake component of the surface water account with level and range of completeness of the reporting . Level of reporting and level of completeness reported for year 2020 (July 2019 to June 2020) of the lake component of the account is provided as the number of lakes for which all the information was provided in full, and number of lakes for which the information was partially reported (in brackets).

Regions	Number of lakes reported in 2020 accounts	Level completeness and range over 1995-2020 [%]	Number of lakes fully and partially (in bracket) reported for 2020
Auckland	11	86.5 [27.5-96.2]	1 (0)
Bay of Plenty	13	91.6 [0-100]	5 (7)
Canterbury	11	94.6 [82.1-100]	3 (3)
Otago	9	98.5 [94.6-100]	6 (3)
West Coast	3	87.1 [82.4-91.4]	1 (1)
Hawkes Bay	1	96.2 [96.2-96.2]	1 (0)
Manawatu	5	50 [0-96.2]	0 (0)
Waikato	13	96.3 [94.9-100]	1 (10)
Wellington	2	48.2 [0-96.5]	0 (1)
Southland	4	99.8 [99.4-100]	4 (0)
Tasman	1	88.2 [88.2-88.2]	0 (0)

2.2.4.3. Hydropower dataset

Changes in the hydropower component between the 2015 and 2020 version of the water accounts are summarised below and are related to: i) changes in the conversion factors between power (M Watts) and flow (cubic metres per second) at some stations; and ii) data availability at the time of the request. The most notable differences include:

1. Bay of Plenty: very poor data availability for both 2015 and 2020 versions.
6. Canterbury: one small station missing in 2020 dataset, and some stations have conversion factor changes.
7. Hawkes Bay: conversion factors changed.
8. Manawatu-Whanganui: no data available in 2020.
9. Marlborough: no data available in 2015.
10. Otago: good data availability for large schemes but no data for small schemes in 2020 (cf. 10-11 up to 2005, none after that in 2015).
11. Southland: good data availability for the dominant scheme, but none for smaller schemes.
12. Taranaki: good data availability for recent years on two schemes in 2020.
13. Tasman: no data in 2020 or 2015.
14. Waikato: as for Otago.
15. West Coast: data available since 2000 for four schemes. No data previously available.

Table 2-3 presents per reporting region a summary of the level of completeness of the information received to complete the hydropower component of the 2020 water accounts.

Table 2-3: Summary of the 2020 hydropower component of the surface water account with level and range of completeness of reporting. Level of reporting and level of completeness reported for year 2020 (July 2019-June 2020) of the hydropower station component of the account provided as the number of hydropower stations for which all the information was provided in full and number of hydropower station for which the information was partially reported (in brackets).

Regions	Number of Hydropower stations in 2020 accounts	Number of hydropower station with no data reported	Level completeness and range over 1995-2020 [%]	Number of Hydropower stations fully and partially (in bracket) reported for 2020
Bay of Plenty	8	4	12 [0-31]	0 (3)
Canterbury	12	2	69 [0-96]	2 (0)
Otago	18	15	12 [0-100]	3 (0)
Hawkes Bay	3	0	90 [78-96]	0 (0)
Waikato	15	3	75 [0-100]	1 (11)
Manawatu	2	2	0 [0-0]	0 (0)
Southland	2	1	48 [0-96]	0 (0)

Regions	Number of Hydropower stations in 2020 accounts	Number of hydropower station with no data reported	Level completeness and range over 1995-2020 [%]	Number of Hydropower stations fully and partially (in bracket) reported for 2020
West Coast	7	2	46 [0-81]	3 (2)
Marlborough	3	0	31 [19-45]	0 (3)
Taranaki	3	1	33 [0-64]	0 (2)
Tasman	1	1	0 [0-0]	0 (0)

3 Water flux

Water flux refers to the flow of water within the water cycle. This includes precipitation (which represents the total water introduced to the land-surface system), evapotranspiration, river flows, and hydro-generation flows.

3.1 Precipitation and evapotranspiration

Figure 3-1 illustrates regional mean annual precipitation and actual evapotranspiration (AET) between 1995 and 2020 (national mean of 530,750 million m^3 and 127,352 million m^3 respectively). It illustrates the large volume of precipitation that falls in the West Coast region compared to other regions. There is less inter-regional difference in AET as it relates more closely to region size rather than climatic patterns. Figure 3-2 and Figure 3-3 show the seasonal pattern of precipitation and AET within each region.

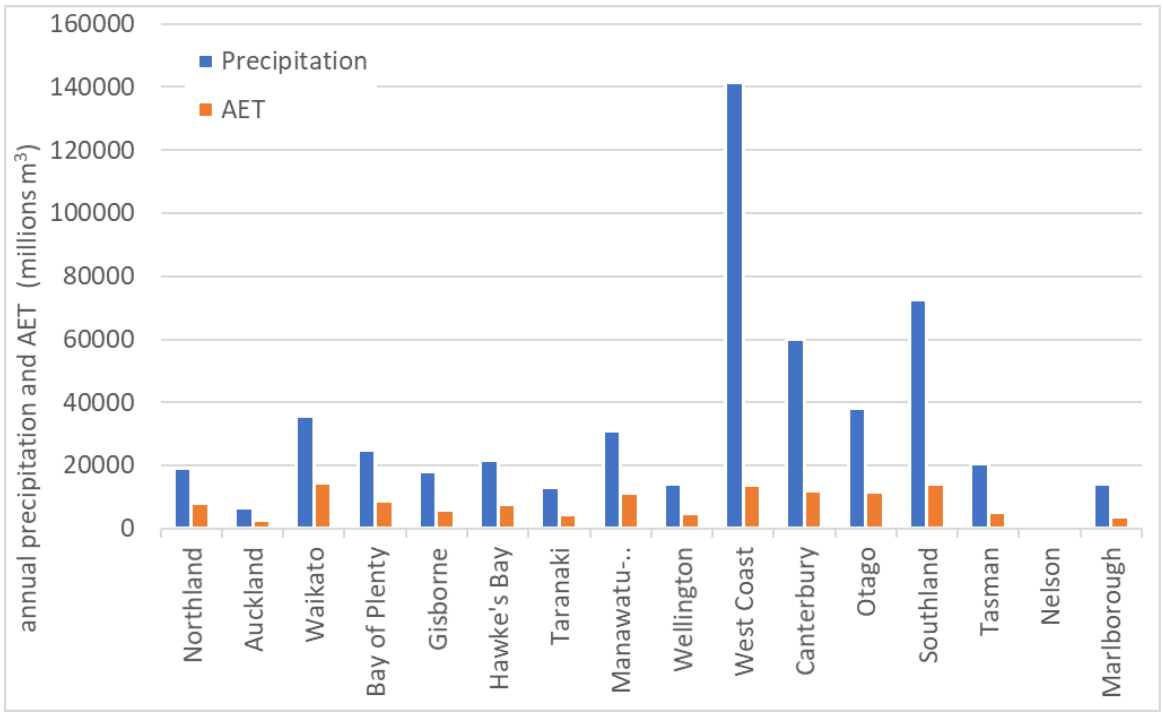

Figure 3-1: Mean annual precipitation and AET (millions m3) by region, 1995-2020.

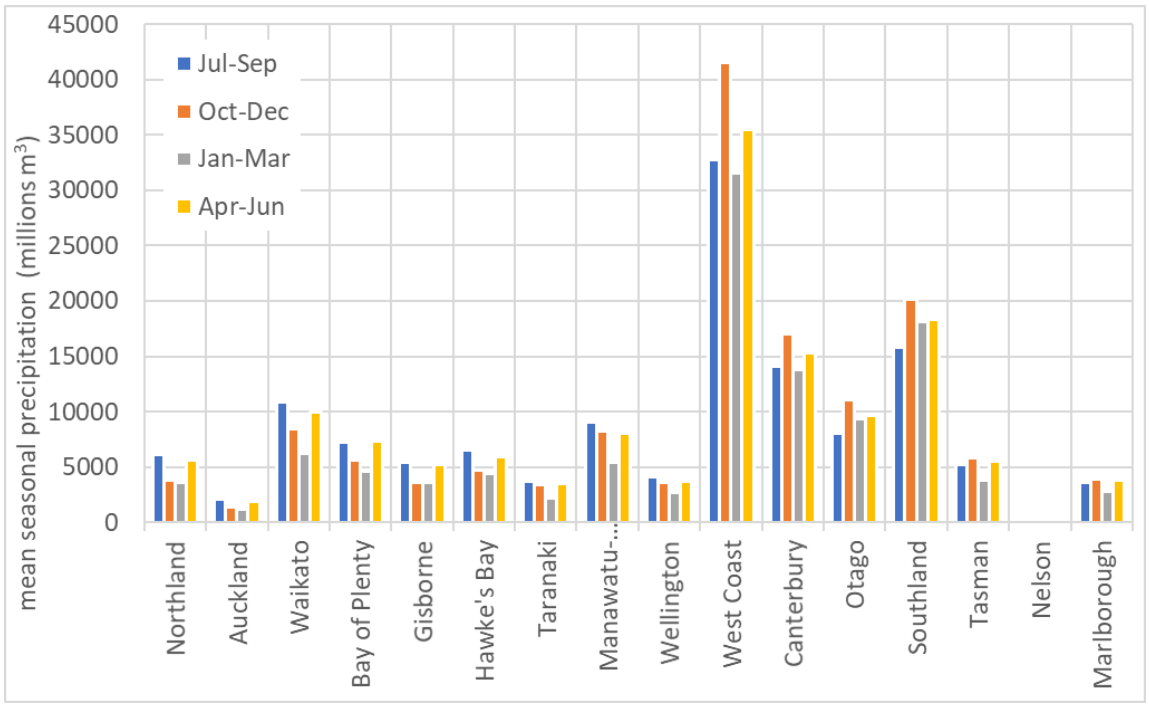

Figure 3-2: Mean seasonal precipitation (millions m3) by region, 1995-2019.

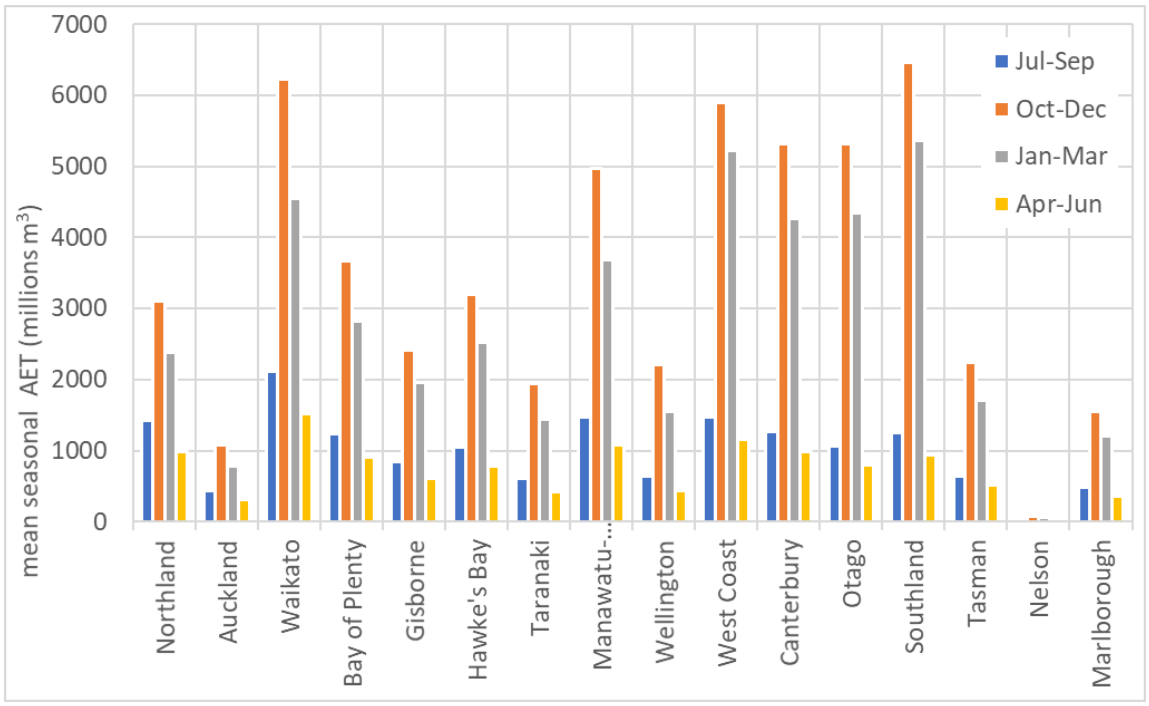

Figure 3-3: Mean seasonal AET (millions m3) by region, 1995-2019.

3.2 River flows

To calculate estimates of river flow, the TopNet model in NZWaM was run across version 2.3 of the New Zealand digital network for hydrological years from 1st July 1985 to 30th June 2020. The period 1985-1994 was a 'warm-up' period for the snow and ice component of the model to reach equilibrium (but was not used within this accounting period). The total mean annual river flows (that eventually flow into the ocean) are illustrated in Figure 3-4. A seasonal break-down of river flows to

the ocean by region (Figure 3-5) indicates that the highest volume of flow to the ocean occurs from the West Coast region.

Mean annual inter-regional river flows (expressed as inflow and outflows) are illustrated Figure 3-6 and **Error! Reference source not found.**. The highest inter-regional flows are from the Canterbury to Otago. Significant flow also occurs from Tasman to the West Coast region, and from Gisborne to Bay of Plenty and Hawkes Bay.

It should be noted that in addition to river flow between regions, water transfer schemes between Manawatu-Wanganui and Waikato (26.77 million m^3/year) and Waikato and Auckland (70.64 million m^3/year) are also included within the totals.

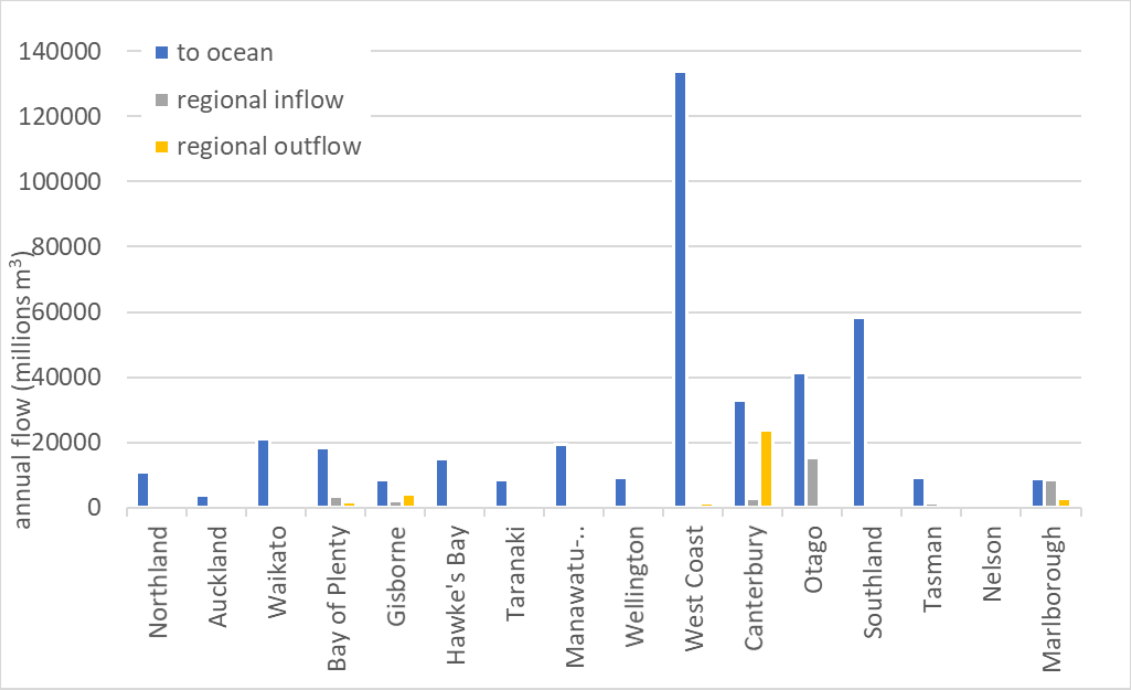

Figure 3-4: Mean annual river flows (millions m3) by region, 1995-2020.

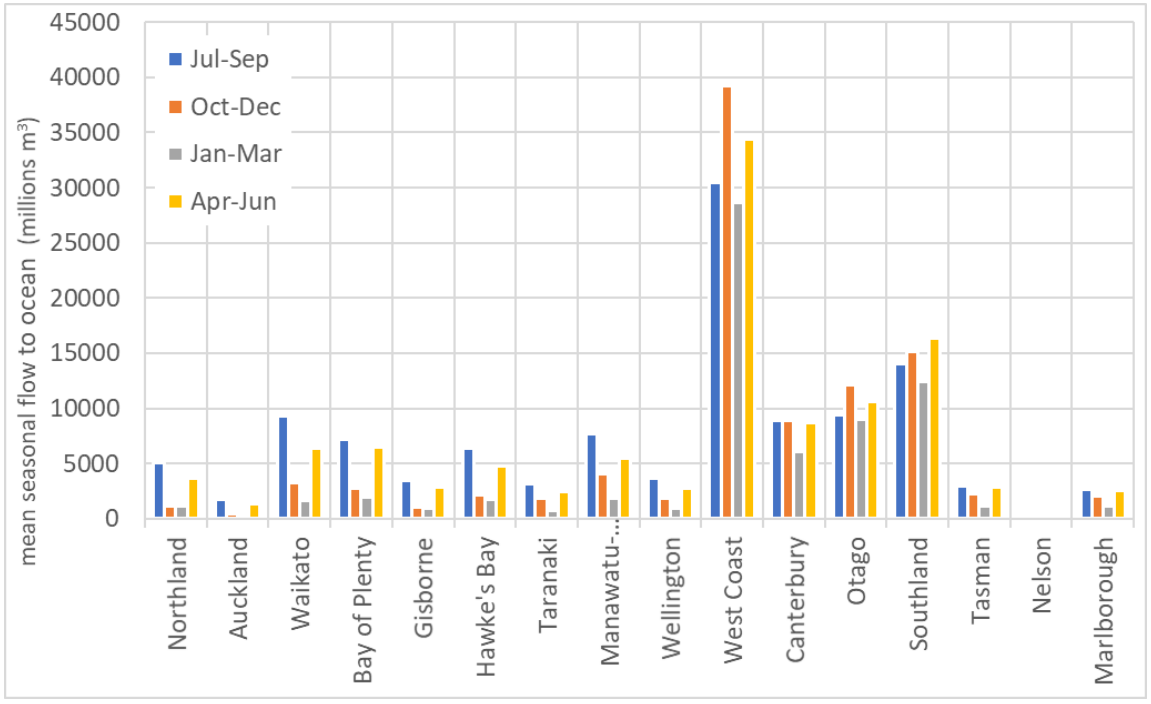

Figure 3-5: Mean seasonal river flow to the ocean (millions m3) by region, 1995-2020.

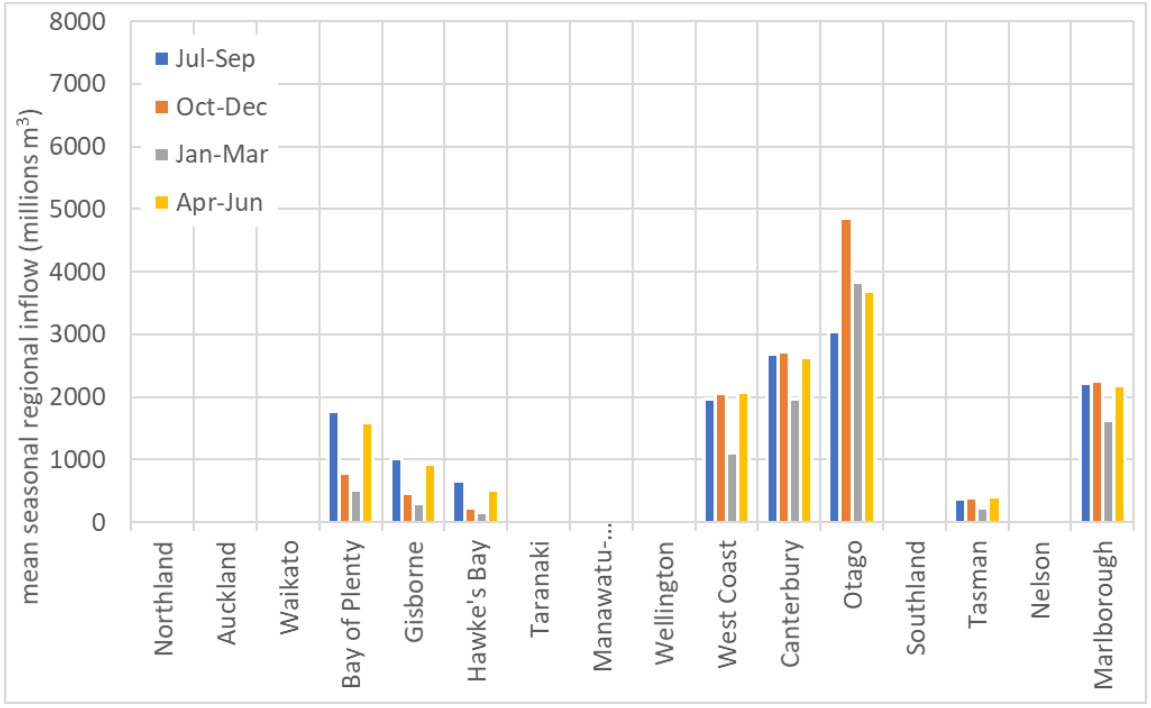

Figure 3-6: Mean seasonal river inflow (millions m3) by region, 1995-2020.

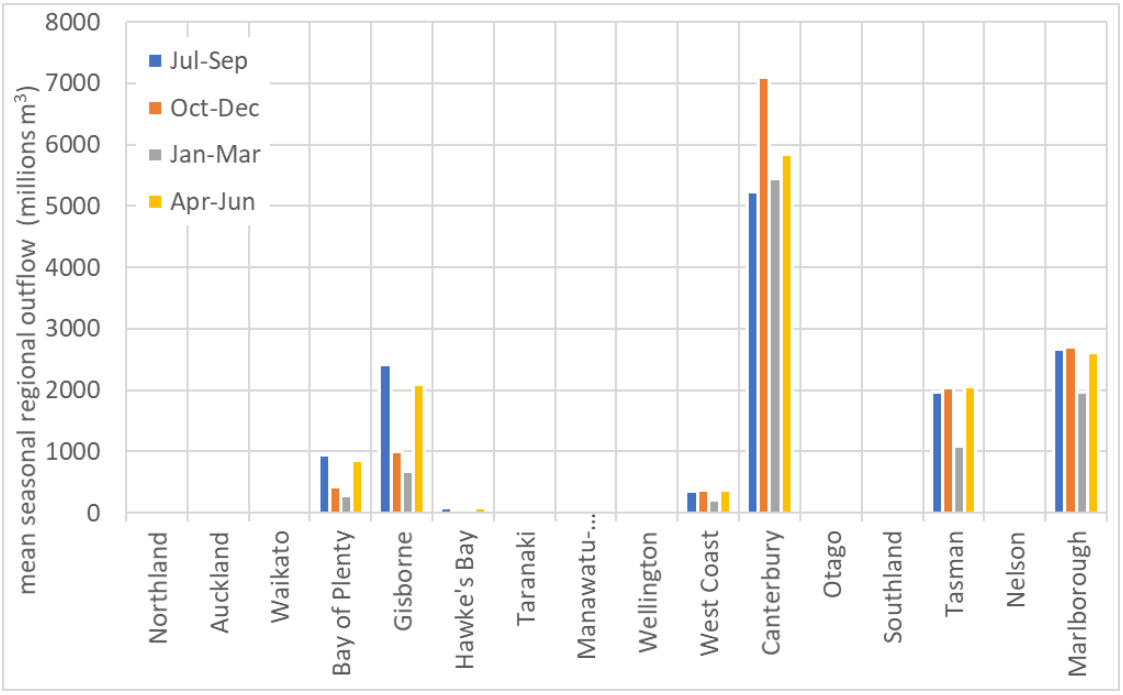

Figure 3-7: Mean seasonal river outflow (millions m3) by region, 1995-2020.

3.3 Hydro-generation flows

Hydro-generation flow describes the amount of water used in hydro-power schemes. Figure 3-8 includes water used in 'run of river' and reservoir hydro-power schemes over the period 1995-2019 (see section 2.2.4) for which water abstracted for use in hydro-power schemes equals water discharged. It should be noted that water volumes may be counted more than once if they pass through downstream power generation stations on the same reach.

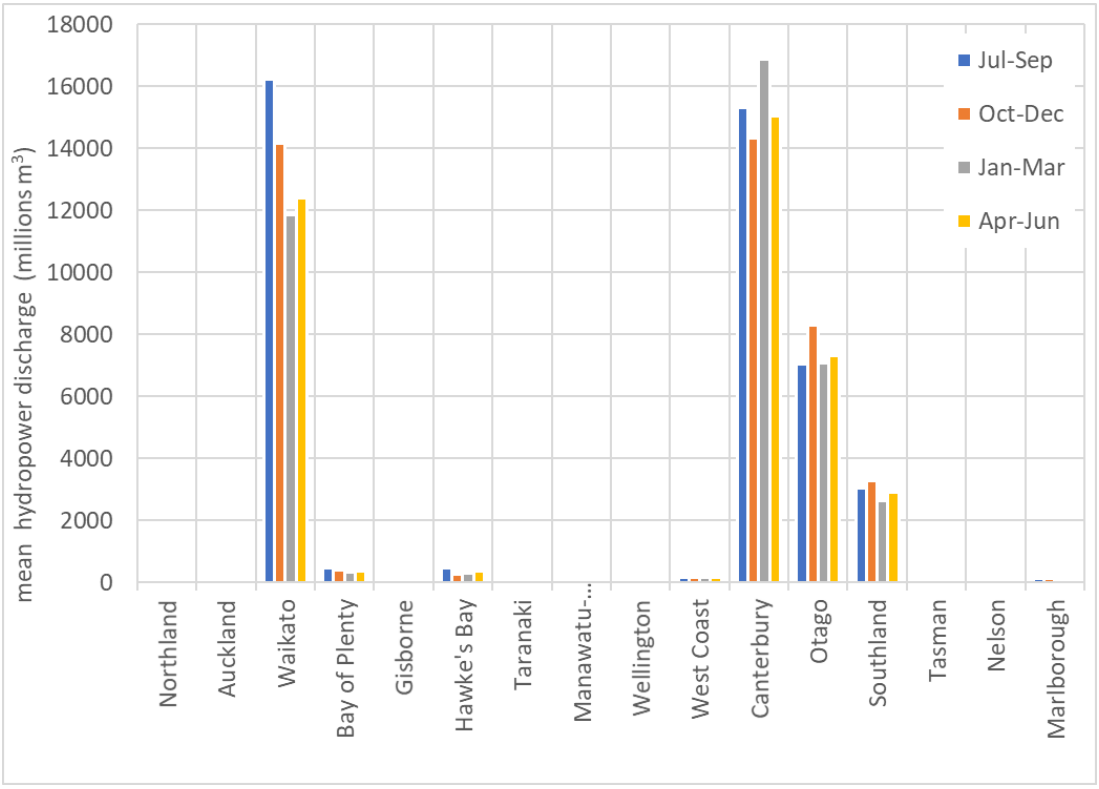

Figure 3-8: Mean hydro-power discharged (millions m3) by region, 1995-2020.

All water storage components show a seasonal variability that is related to seasonal climate variability. Variability within the period 1995 to 2020 is discussed below.

3.4 Soil moisture, snow and lake and reservoir storage

Figure 3-9 and Figure 3-10 illustrate the mean annual change in soil moisture and snow water storage by region, for the period 1995 to 2020, while Figure 3-11 illustrates the mean annual change in lake storage over the period 1995-2019 (see section 2.2.4). The change in water storage variables are calculated as the difference between successive beginnings of time periods. The annual change in soil moisture storage for example, is calculated as the difference in soil moisture between the first day of each hydrological year and the subsequent hydrological year. Similarly, the change in soil moisture for each season is calculated as the difference between soil moisture at the start of one season and the start of the subsequent season (so change in soil moisture for the last season (4) of 2010 (April-June 2011), is the soil moisture on 1 July 2011, minus the soil moisture on 1 Apr 2011).

It can be seen from Figure 3-9 that total moisture stored in soil increases most from the start of April to the end of June (Autumn) and decreases most from October to December (Spring). As expected, total volume change in soil moisture change are related to region size.

By contrast, significant change in snow storage occurs only in the West Coast, Canterbury, Otago and Southland regions (Figure 3-10). Similarly, mean annual change in lake and reservoir storage is significant only in Canterbury and Otago regions (Figure 3-11).

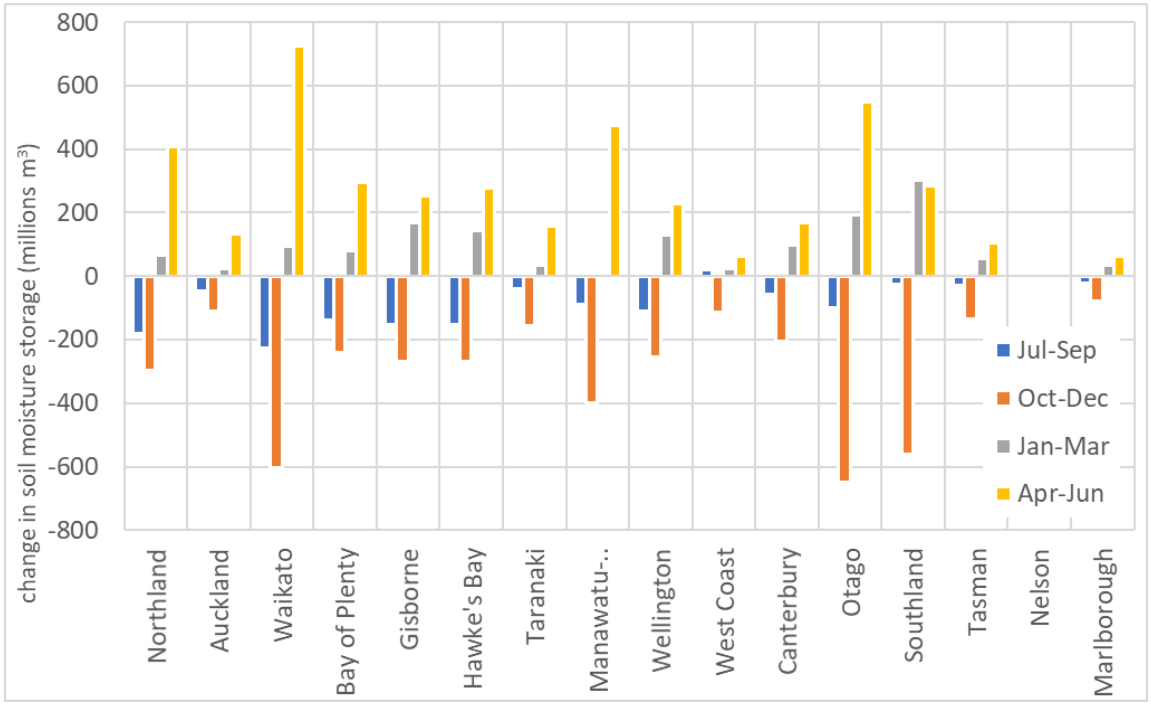

Figure 3-9: Mean seasonal change in soil moisture water storage (millions m3) by region, 1995-2020.

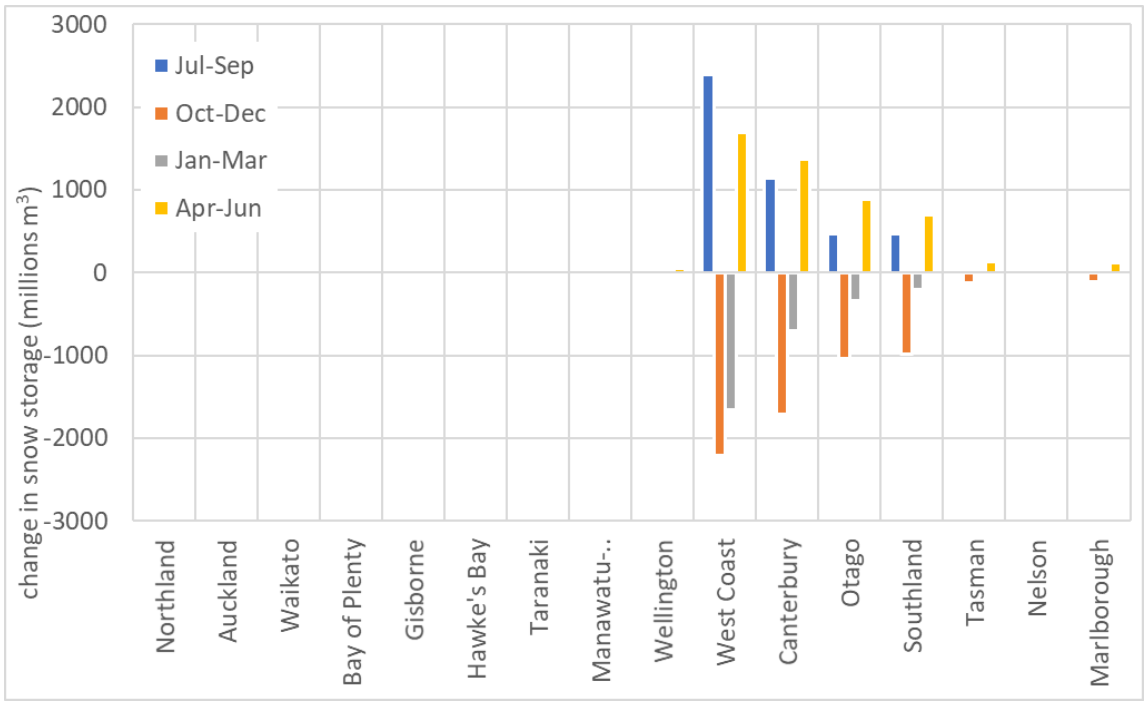

Figure 3-10: Mean seasonal change in snow water storage (millions m3) by region, 1995-2020.

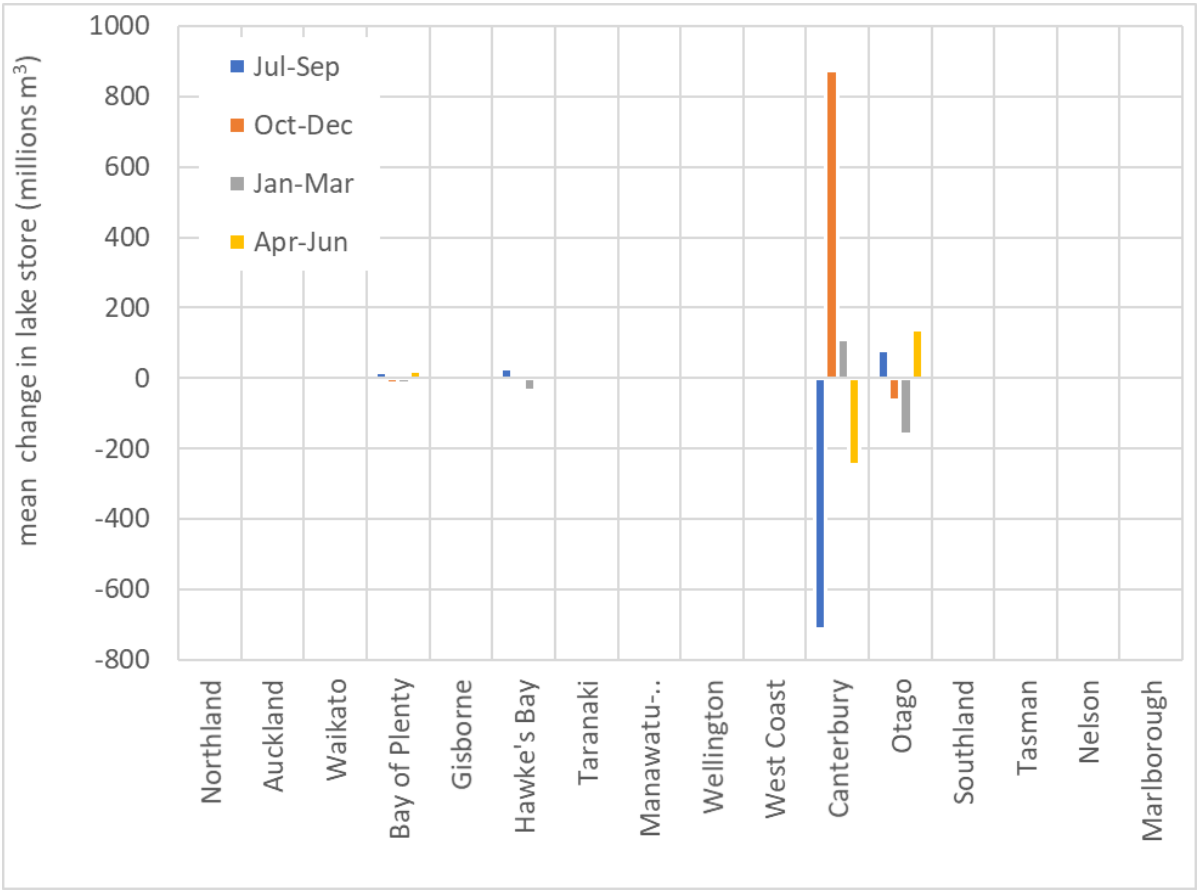

Figure 3-11: Mean seasonal change in lake and reservoir water storage (millions m3) by region, 1995-2019.

3.5 Ice storage

Analysis of ice data storage is based on observational data and is limited to regions that hold glaciers. A normalised master snowline altitude series for the Southern Alps has been created from glaciers that have been monitored since the late 1970s. All glacier snowline altitude estimates were converted to standard deviation units relative to the 1981-2010 average altitude to show interannual snowline departures for each glacier. Then those values were averaged to create a master series (Figure 3-12). A check of the climatological average altitude for 1981-2010 relative to the starting snowline altitude for 1977 indicates a positive elevational shift of ~20m +/-13m, which is consistent with warming temperatures. An additional comparison for glaciers in different subregions of the South Island shows the snowline response regionally robust (Figure 3-13). The similarity of the inter-regional snowline altitude signature suggests a Southern Alps master snowline series can be used to evaluate the long-term response of the wider glacierised area over the South Island to climatic variability and change.

At present, there are in situ mass balance measurements gathered for Rolleston Glacier (located in north Canterbury, Arthur's Pass) and Brewster Glacier (located in Mt Aspiring National Park) twice a year. Largely speaking, the inter-annual patterns and mean values for annual mass balance change (in meters of water equivalent volume) at both sites are similar. Given the similarity of the snowline response across all subregions (and sites therein) for the Southern Alps, we consider Brewster and Rolleston observed mass balance changes representative of the wider region. A combined series for Brewster and Rolleston annual mass balance was created for 2011-2019 and plotted in a linear regression with normalised snowline values. The resulting regression equation offers an opportunity

to transform Brewster and Rolleston normalised snowline altitude values to estimate long-term changes in hydrological balance and ice volume.

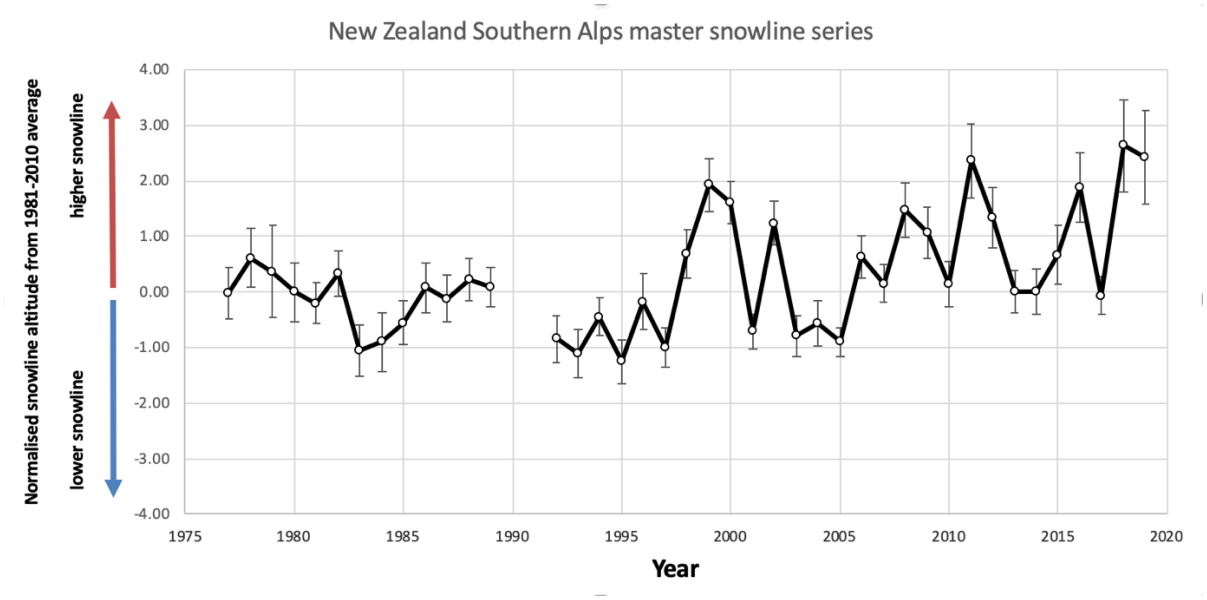

Figure 3-12: New Zealand Southern Alps master snowline series showing the normalised departure of the end of summer snowline. Altitude relative to the 1981-2010 average position. Data are from the most recent report on the NIWA End of Summer Snowline mission.

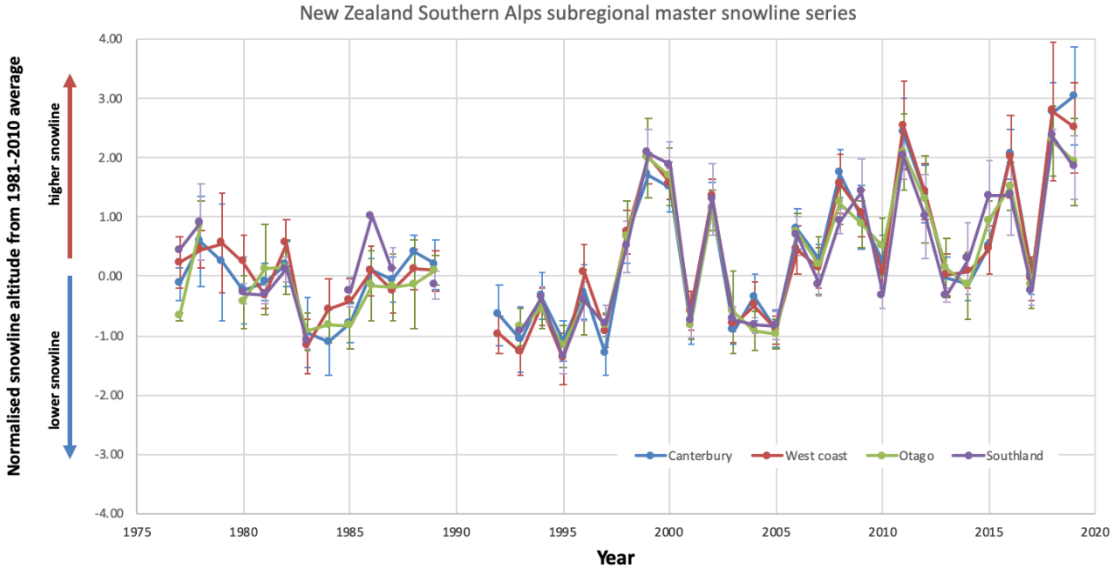

Figure 3-13: New Zealand Southern Alps sub-regional master snowline series. showing the similarity in the normalised departure of the end of summer snowline altitude relative to the 1981-2010 average position across different areas of the South Island.

The time series of ice on Rolleston Glacier (Figure 3-14) illustrates that a positive ice mass balance dominates the winter season when snow falls, while negative mass balance typifies the summer months when melt is high. The relatively poor winter mass balance season in 2018 was followed by a poor summer 2018 season made that year one of the worst overall mass balance years for this glacier and others across the Southern Alps. This pattern is expected to increase in frequency under climate change.

The observed pattern of cumulative mass change, which aggregates both winter and summer mass balance impacts, was replicated between Rolleston Glacier (located in north Canterbury, Arthur's Pass) and Brewster Glacier (located in Mt Aspiring National Park) (Figure 3-15). The overall trend since 2010 has seen both glaciers experience a decline in mass balance through the 2019 glacier year (ending March 2019). Rolleston recorded a -6.2 m water equivalent loss and Brewster recorded -5.6 m water equivalent loss during this time. The trend for both seasonal mass balance components suggests a shift toward reduced winter snowfall and warmer summer temperatures resulting in about -0.5 m water equivalent per year in each of the main winter/summer seasons). This has had dually significant impacts on the net mass balance (now about -1 m water equivalent per annum, achieved by the end of the most recent observational decade).

Elaboration of the methods used in collection of these data is given in Appendix C.

The values from the estimated interannual meter water equivalent (m.w.e.) change time series were combined with a joint surface area estimate for Brewster and Rolleston of 296.5 ha in 1978 in order to create a cumulative aggregated change time series for water storage for those two glaciers combined. This approach is rudimentary; it does not take glacier surface area change into the frozen water account and is therefore considered provisional and conservative. It may be more difficult to apply this type of method to larger, more complicated glaciers or to glaciers in other regions of New Zealand.

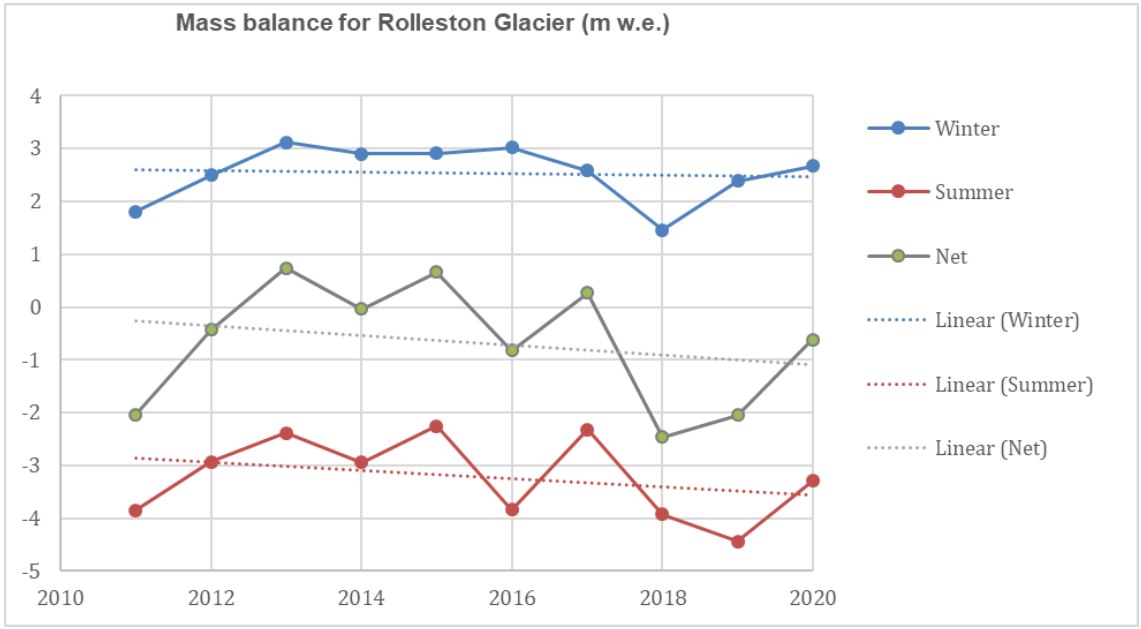

Figure 3-14: Mass balance Index (meters water equivalent) measurements (winter, summer, net) since 2010 from Rolleston and Brewster glacier. Winter measurement for Brewster glacier to be updated; summer survey not available due to COVID-19 lockdown. Dotted lines indicate linear regression line for each dataset.

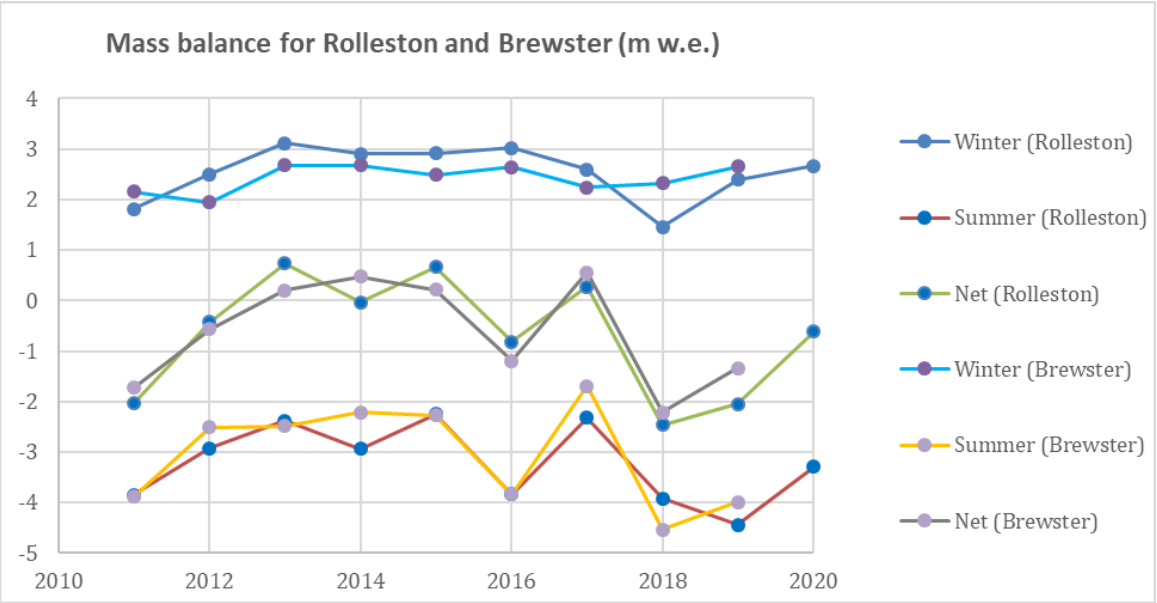

Figure 3-15: Mass balance (meters water equivalent) measurements (winter, summer, net) since 2010 from Rolleston and Brewster glacier using in situ. Monitoring undertaken by University of Canterbury, University of Otago and Victoria University Wellington. Winter measurement for Brewster glacier to be updated; summer survey not available due to COVID-19 lockdown.

However, an overall reduction from 94.32 million m^3 water volume in 1978 to 57.09 million m^3 water volume in 2019 (total reduction of 37.23 million m^3) was calculated using this new method, and it suggests only 61% of the total water resource formerly held in ice in 1978 for Brewster and Rolleston combined existed at the end of the 2018/19 season (Figure 3-16). The change from 2016 to 2019 that was also calculated using this approach indicates a significant loss of ~15.65 billion litres of water during that short but accelerated melt interval (40% of the total lost since 1978), which compares well to an estimate of ~13 billion litres lost derived from geodetic modelling using structure from motion photogrammetry.

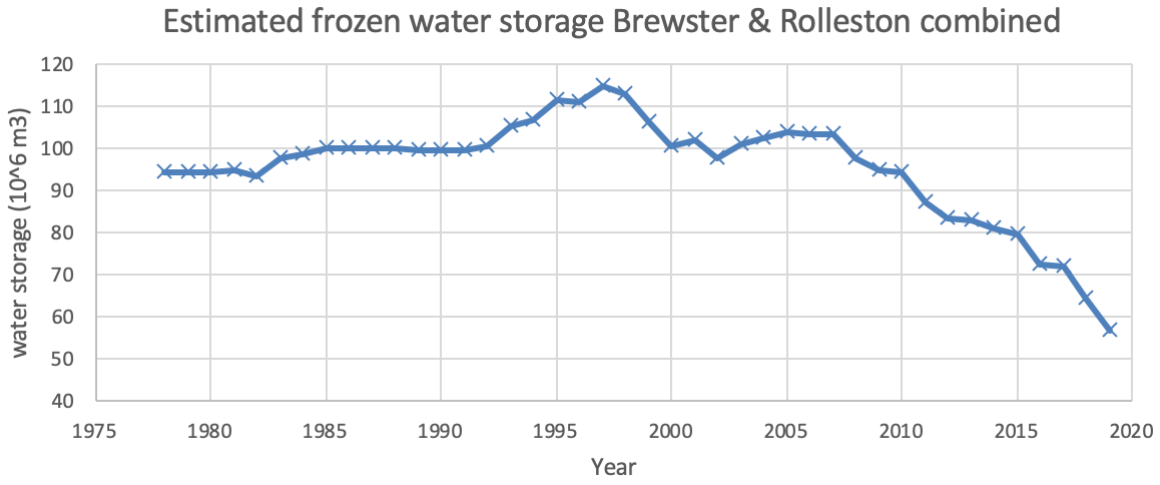

Figure 3-16: Estimated frozen water storage (in m.w.e.) for Brewster and Rolleston Glacier combined between 1978-2019. utilising the starting surface area for both glaciers combined and the iteratively adjusted time series of interannual m.w.e. change.

When applying the reduction of 12.39 m.w.e to the total glacierized surface area of the wider Southern Alps, a total potential volume of water and ice lost to the region can be estimated. This approach to calculating the change is also rudimentary and provisional at best and recognises that much more work is still required to make further estimates of change for individual glaciers and for individual regions. Nevertheless, it conservatively estimates ~70.5% of the ice formerly catalogued for the Southern Alps in 1978 remained at the end of the 2018/19 season (Table 4-1). When the same percentage of loss is applied to discrete geopolitical regions of the South Island (Table 4-2 and Figure 3-17), it is clear that some areas (such as Marlborough, Southland, and Otago) are nearly at the point of total loss or close to losing all of their ice.

Table 3-1: Calculation of total ice volume reduction for the Southern Alps of New Zealand. using the total m.w.e. reduction estimated at Brewster/Rolleston glaciers applied to the total glacierized surface of the South Island as of 1978.

Area of glacier coverage	1978 areal extent (ha)	Initial volume estimate (km^3)	Water volume equivalent lost over glacierized area (km^3)	Ice volume lost	% ice lost since 1978
Southern Alps	115336	53.81	14.29	15.72	29.5

Table 3-2: Calculation of total ice volume reduction for subregions of New Zealand's South Island. using the total m.w.e. reduction estimated at Brewster/Rolleston glaciers applied to the total glacierized surface each region as of 1978.

Region	1977/78 ice volume (km^3	Post 2018/19 ice volume (km^3)	Est. minimum volume lost (km^3
Canterbury	27.8812	19.6563	8.225
Marlborough	0.0068	0.0048	0.002
Otago	3.1062	2.1899	0.9163
Southland	0.9366	0.6603	0.2763
West Coast	21.8799	15.4253	6.4546
Total South Island	53.8108	37.9366	15.8742

To interpret that above figures in a manner more compatible with the other data sources described in this report, the interannual percentage of ice volume change based on the observations for Brewster/Rolleston (in West Coast region), was applied to other regions that exhibit glacial water storage (Figure 3-17). As a result of this approach, the proportion of total glacial water resource in each region remains constant.

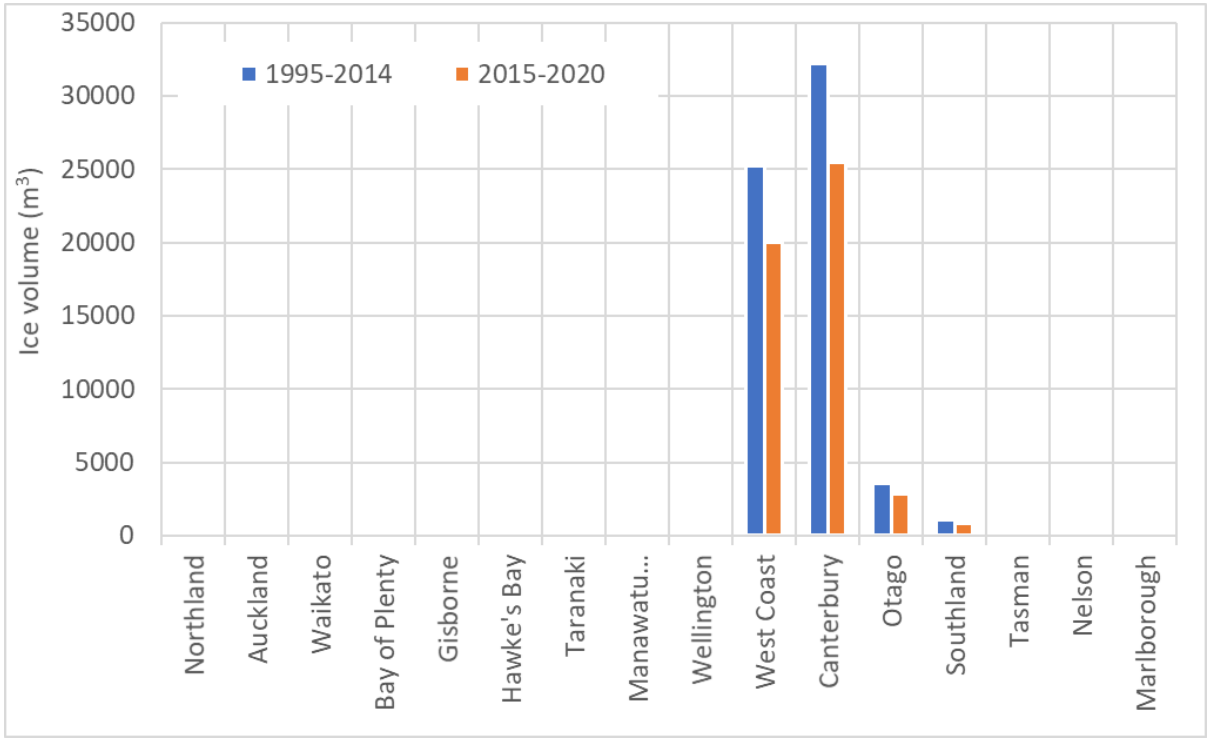

Figure 3-17: Average water volume stored as ice in each region for the periods 1995-2014 and 2015-2020.

4 Discussion

4.1 Variability

Figure 4-1 and Figure 4-2 illustrate the temporal variation in annual water flux and storage respectively. Inter-annual variability in total precipitation (and thus total river outflows to the sea) has decreased in the last five years. Over the same period, whilst full hydro-power flow data for the 2020 were unavailable and have been omitted, there has been a gradual increase in hydrogeneration. Inter-annual variability in water storage change also appears to have decreased in the last five years, though both these trends would need to continue for a greater number of years before they become statistically significant. The last five years have been noticeable for marked reductions in snow storage.

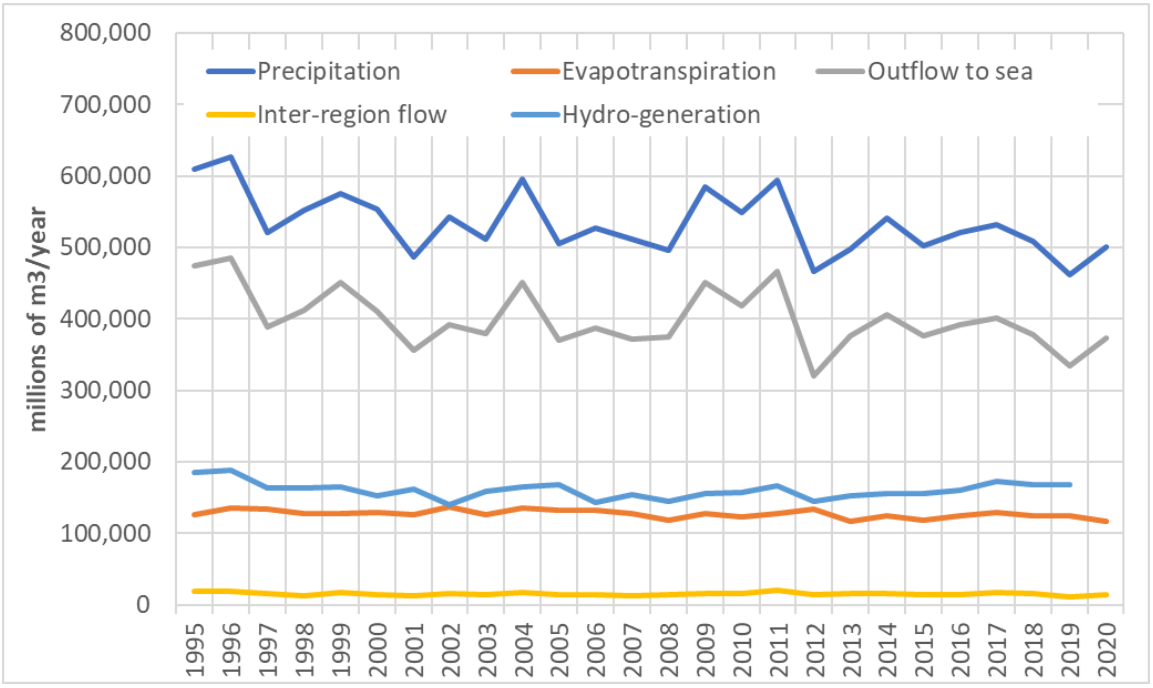

Figure 4-1: Variation in total annual water flux (millions m3) from 1995 to 2020.

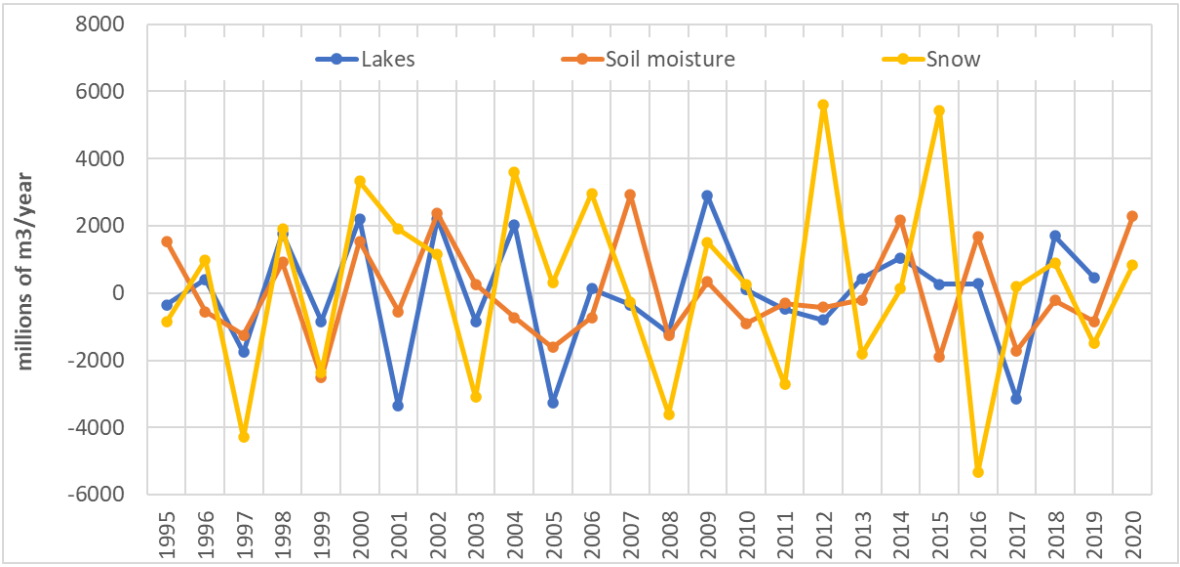

Figure 4-2: Variation in total annual water storage (millions m3) from 1995 to 2020. lake data to 2019 as 2020 record is incomplete.

4.2 Observation data and model reliability

The above estimates of water fluxes and storages within New Zealand are based on available observation data and model output. However, some uncertainty exists in all observation data and model output. The rainfall data from the Virtual Climate Station Network (VCSN), that drives the surface water component of NZWaM (TopNet) for example, is interpolated from data supplied by rain gauges across New Zealand. The total number of reporting rain-gauges may differ on any given day (due to mechanical breakdown). If the number and distribution of working rainfall gauges changes, we would expect the interpolated rainfall to change; and as a result, predictions from the model to change. The availability and reliability of observation data then, will have an unspecified impact on both the seasonal and year to year variability predicted in the water accounts. It is worth noting at this point that for the most recent reporting period, data availability has generally increased. For example, over 90% of identified lakes had data available for inclusion in accounting every month (with 100% available for 215 out of 288 months; and over 95% of data available for 276 out of 288 months).

A comparison of mean annual water fluxes and storage change reported in previous studies (e.g., the previous water account report) can be used as a simple indictor of the potential impact of this type of data uncertainty on the water accounts (and also bring attention to the unwritten assumption of climate stationarity during the study period).

Table 4-1 illustrates precipitation, evapotranspiration and runoff estimates made in the literature and the previous water accounting report (Collins et al. 2015). Whilst mean national precipitation in this study (2026 mm/year) compares well with previous studies, modelled evapotranspiration is low (486 mm/year) compared to Toebes (1972) and Woods and Henderson (2003).

Similarly, we know that the representation and parametrisation of the evapotranspiration model has improved since the last water accounting report. So, as this study predicts higher evapotranspiration that the previous report (all other processes representation stayed the same), we can say that previous estimates of runoff were likely over-predicted.

Table 4-1: Water balance estimates for New Zealand from previous studies.

Study	Precipitation (mm/year)	Evapotranspiration (mm/year)	Runoff (mm/year)
Toebes 1972	2059	599	1481
Woods and Henderson 2003	1515	639	808
Woods et al. 2006	1884	683	1365
Henderson et al. 2007	2106	427	1664
Henderson et al. 2011	2321	453	1869
Collins et al. 2015 Water accounts report	2130	391	1675
This accounts report	**2026**	**486**	**1516**

Table 4-2 illustrates the mean annual water flux and storage values for current reporting period compared to the previous period. As there is an overlap in reporting periods (1995 to 2014) the variability of different water flux and storage during the last five years (as indicated in the above section) is masked by mean annual figures over the whole period.

Table 4-2: Summary of mean annual water flux and storage amounts for the accounting periods 1995-2014 and 1995-2020.

Component	1995-2014 (millions of m^3 /year)	1995-2020 (millions of m^3 /year)
Precipitation	542,536	533,771
Evapotranspiration	128,583	127,310
Outflow to sea	407,384	400,159
Inter-regional flow	15,724	15,500
Hydro-generation	159,586	160,092[2]
Change in lake storage	0.7	-69[3]
Change in soil moisture storage	52	12
Change in ice storage	-842	-1121
Change in snow storage	233	200

[2] Calculated over the period 1995-2019
[3] Calculated over the period 1995-2019

A more comprehensive discussion of the uncertainty associated with the TopNet model used in NZWaM is given by Booker and Woods (2014).

4.3 Validation

As direct verification of regional-scale prediction made in the water accounts is not possible (there being no single gauge for the whole region), prediction validation can be approached in a number of ways.

Figure 4-3 for example, shows the correlation of interpolated regional-scale rainfall (VCSN data) compared to observed rainfall in Auckland, Waikato, Wellington and Taranaki. There is a good correlation between each of the datasets and their regional mean – indicating that the pattern of interpolated regional rainfall is spatially consistent with the observed data. There is however, a strong bias indicated because a greater number of observed data gauges tends to be located in more easily accessible urban centres which also tend to have lower rainfall than more remote locations. This bias then decreases the regional estimates.

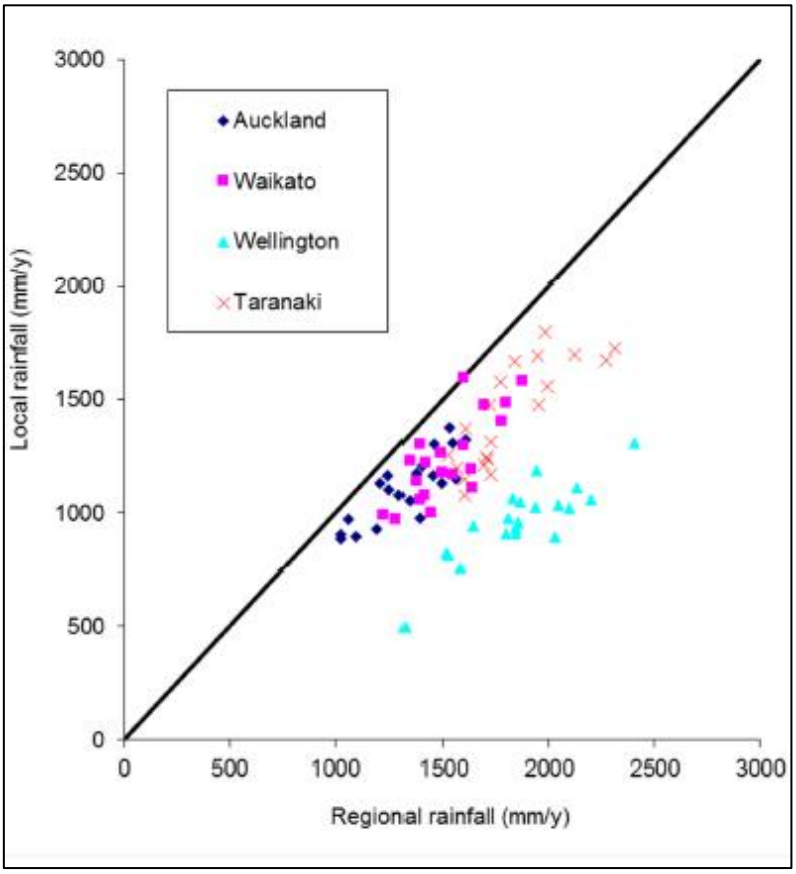

Figure 4-3: Comparison of annual local rainfall gauge data with regional VCSN data. Comparison of annual local rainfall gauge data with regional VCSN data for Auckland, Waikato, Wellington and Taranaki.

A similar comparison was made for river flow data. Figure 4-4 shows that there is a good relationship between the West Coast region seasonal surface water flow volume with the total volume of flows from two of the largest rivers in the region (Haast and Buller). Even the relationship between total region volume and a single catchment (the Haast) is identifiable albeit less strong (R^2 = 0.5718 compared to R^2=0.7284).

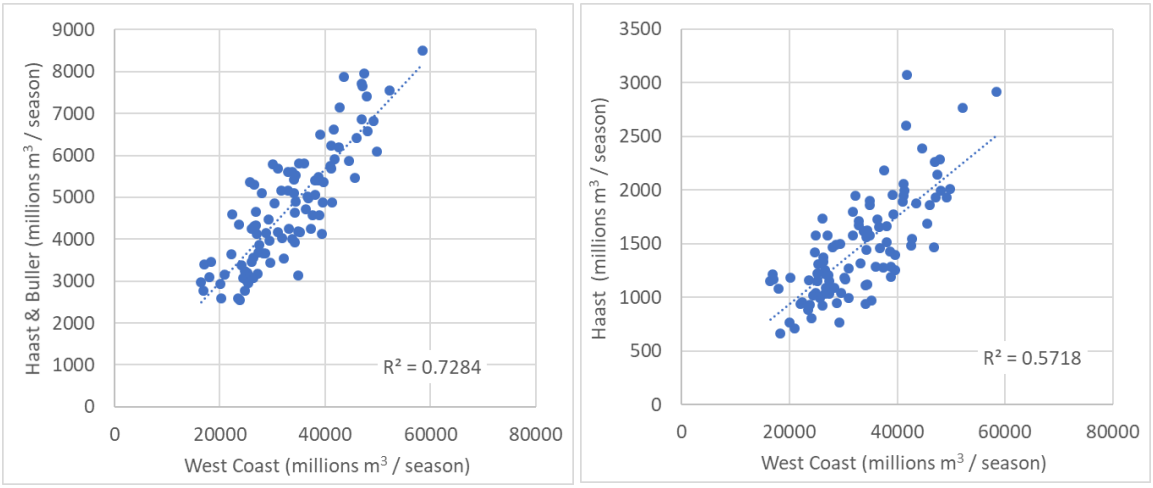

Figure 4-4: Comparison of West Coast region seasonal surface water flow volume . Summed Haast and Buller catchment flow volume (left), and the Haast catchment flow volume (right).

Finally, Figure 4-5 shows the comparison for water crossing the regional boundary between Tasman and West Coast, compared to the flow record from Buller at Longford, which represents about one third of the area involved. The relationship between annual flows is strong, and the multiplier is of the right order.

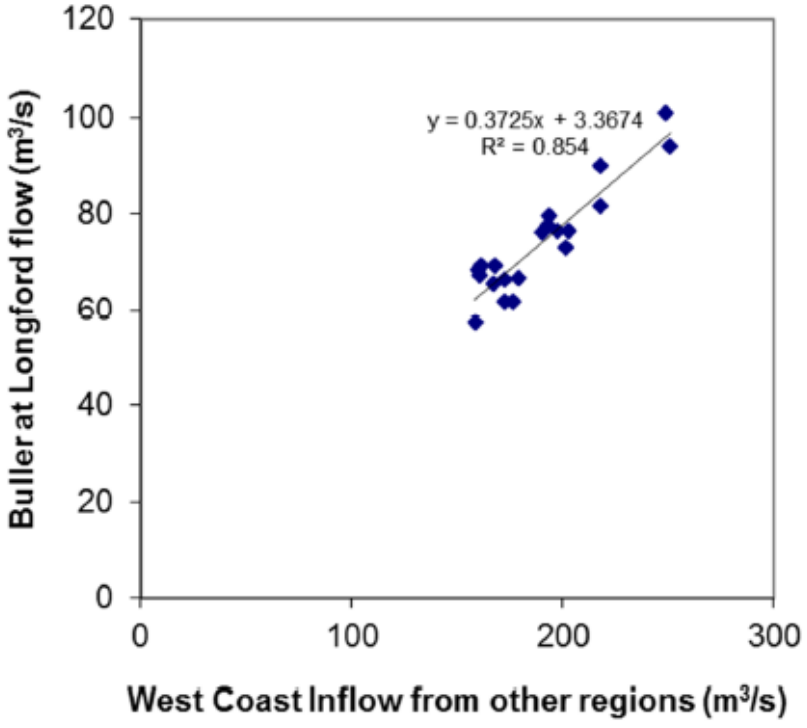

Figure 4-5: Runoff from Tasman District to the West Coast region.

5 Summary

Eleven components of the hydrological cycle in New Zealand (seven flows and four storages) have been analysed and described at a national and regional scale for the period 1995-2020. The water accounts capture the broad temporal and regional variability of water movement and storage. The analysis shows that precipitation, river flows to the sea, and evapotranspiration are major components of the water cycle. It has also been shown that abstraction/discharge by hydro-generation is a substantial non-consumptive use of water.

It has been noted that whilst there is uncertainty in both observed data and model analysis, validation checks of the dominant sources of input and output data (precipitation and river flows respectively) provides confidence in the presented results.

6 Acknowledgements

We acknowledge the following sources of information used in the preparation of these accounts. The following organisations have given permission to use their data, and/or helped make it available:

Hydro-generation data:

Contact Energy Ltd
Genesis Power Ltd
Meridian Energy Ltd
Mercury Energy Ltd
TrustPower Ltd

Lake level data:

Auckland Council
Alpine Energy & Environmental Consultancy Services
Bay of Plenty Regional Council
Canterbury Regional Council
Contact Energy Ltd
NIWA (funded by NIWA under Environmental Information Programme 1 (2014/15 SCI))
NZX
Genesis Energy Ltd
Meridian Energy Ltd
Mercury Energy Ltd
Otago Regional Council
TrustPower Ltd
Waikato Regional Council
Greater Wellington Regional Council
WaterCare Ltd

7 References

Booker, D.J. and Woods, R.A. (2014) Comparing and combining physically-based and empirically-based approaches for estimating the hydrology of ungauged catchments. Journal of Hydrology, 508, pp.227-239.

Collins, D. Zammit, C, Willsman, A., Henderson, R.D. (2015) Surface water components of New Zealand's National Water Accounts, 1995-2014, NIWA CLIENT REPORT No: CHC2015-013-v2

Feddes, R. A., Kowalik, P., & Zarandy, H. (1978). Simulation of field water use and crop yield. Wageningen, the Netherlands: Pudoc.

Henderson, R.D., Woods, R., Singh, S., Zammit, C. (2011) Surface water components of New Zealand's National Water Accounts, 1995-2010. *NIWA Client Report CHC2011-051*: 45.

Henderson, R. D., Woods, R.A., Tait, A.B. (2007) Surface water components of New Zealand's National Water Accounts. *NIWA Client Report CHC2007-046*: 40.

Toebes, C. (1972) "The Water Balance of New Zealand." *J Hyd (NZ) 11*(2): 127-139.

Woods, R.A., Henderson, R.D. (2003) Surface water components of New Zealand's National Water Accounts, 1995-2001. *NIWA Client Report No. CHC2003-074*: 50.

Woods, R. A., Hendrikx, J., Henderson, R.D., Tait, A.B. (2006) "Mean Flow Hydrology of New Zealand Rivers." *J Hyd (NZ)* ***45***(2): 95-110.

Yang, J., McMillan, H., Zammit, C., (2017) Modelling surface water–groundwater interaction in New Zealand: model development and application. Hydrological Processes, 31(4), pp.925-934.

Appendix A Regional data used

Region Name	Region Area (km^2)
Auckland	4,354
Bay of Plenty	11,939
Canterbury	44,915
Gisborne	8,452
Hawke's Bay	14,090
Manawatu-Wanganui	22,198
Marlborough	10,126
Nelson	393
Northland	11,838
Otago	31,828
Southland	29,529
Taranaki	7,196
Tasman	9,548
Waikato	24,320
Wellington	8,012
West Coast	23,204
New Zealand	**261,944**

Appendix B R scripts descriptions

These scripts were prepared for Stats NZ to summarise various TopNet output variables over time (annual and seasonal) and over space (regional). The variables summarised are: flow to the ocean, flow between regions, precipitation, evaporation, change in soil moisture, and change in snow.

Inputs

The scripts need the following input files:

16. The 16 TopNet spatial files, one per TopNet region, at Strahler level 3;

17. The 16 TopNet streamq files, one per TopNet region, each containing the variables: area, area_elev, snwstor_elev, aprecip, canevap, snowevp, soilevp, river_flow_rate_mod, and soilh20.

18. The csv file, DN2_strahler3_reporting_and_discharge.csv, which has three columns: reach ID, reporting region, and discharge region. The reach ID is the Strahler 3 aggregate catchment reach ID, the reporting region is the Stats NZ region (1 to 16) that the catchment is mostly in (this is often the TopNet region, but the boundaries are slightly different), and the discharge region which is the Stats NZ region that the catchment discharges into (it is -1 if it is the same as the reporting region).

Hydrological year and seasons

The variables are summarised annually and seasonally. The year is taken to be the hydrological year, the beginning of the year and the four seasons are summarised in this table:

Season	Begins
1	00:00 1 July
2	00:00 1 Oct
3	00:00 1 Jan
4	00:00 1 Apr

In the seasonal output files columns will be headed up in the format year.season. For example, 2008.2 would indicate that value is for the 2nd season in 2008 (00:00 1 Oct 2008 to 23:00 31 Dec 2008).

Summative variables (such as precipitation) are summed from the beginning of the time region to just before the end. For example, precipitation for 1998 is the sum of the precipitation from 00:00 1 July 1998 to 23:00 30 June 1999. Difference, or change, variables (such as change in soil moisture) are calculated using the difference between successive beginnings of time periods. For example, the change in soil moisture for 2010.4 (remember this is in 2011 calendar year) is the soil moisture at 00:00 1 July 2011 minus that at 00:00 1 Apr 2011.

Requirements

These are R scripts, they were tested on version 3.6.2. The only libraries needed are ncdf4 and stringr. Due the large streamq input files the scripts need about 20G of RAM to run.

Process

There are five scripts: misc.r, snwstor.r, national_annual_and_seasonal.r, regional_annual_and_seasonal.r, and csvs.r. The misc.r has a couple miscellaneous functions that the other scripts need; you don't need to run it directly, but you do need to edit it as follows:

1. Edit the misc.r script setting the base, streamq_path, spatial_path, sq_head, and sq_tail variables near the top. These variables allow the rest of the scripts to find the input files.

2. The first script to run is snwstor.r. This script generates the snwstor*area array from the snwstor_elev and area_elev variables and stores it in snwstor.RData. This variable is needed by the rest of the scripts, but is not in the default streamq TopNet files. This script doesn't use a lot of RAM and should take a few minutes to run.

3. The main script is national_annual_and_season.r. This reads the hourly TopNet streamq files (and the snwstor.RData file) and aggregates the variables annually and seasonally. The variables output are: Q (flow), P (precipitation), AET (evaporation), DeltaSM (change in soil moisture), and DeltaSnow (change in snow). All variables give the value per reach. Q, P, AET have been summed over the year (or season); DeltaSM and DeltaSnow are the differences over the year (or season). The files generated are: Q_Annual.RData, P_Annual.RData, AET_Annual.RData, DeltaSM_Annual.RData, DeltaSnow_Annual.RData, Q_Seasonal.RData, P_Seasonal.RData, AET_Seasonal.RData, DeltaSM_Seasonal.RData, and DeltaSnow_Seasonal.RData

4. You can run it using R script national_annual_and_season.r. This script uses about 20G of RAM and will take a couple hours to run.

5. regional_annual_and_seasonal.r reads the annual and seasonal files from the previous step and does the spatial aggregation into regions. It uses the csv file, DN2_strahler3_reporting_and_discharge.csv to determine which region each reach belongs to, and also which region it discharges to. The variables outputted are: Ocean (flow to the ocean), Out (flow out of a region into another region), In (flow into a region from other regions), P, AET, DeltaSM, and DeltaSnow. All variables give the values per region, annually and seasonally. The files generated are: Ocean_Ann_Reg.RData, Out_Ann_Reg.RData, In_Ann_Reg.RData, P_Ann_Reg.RData, AET_Ann_Reg.RData, DeltaSM_Ann_Reg.RData, DeltaSnow_Ann_Reg.RData, Ocean_Seasonal_Reg.RData, Out_Seasonal_Reg.RData, In_Seasonal_Reg.RData, P_Seasonal_Reg.RData, AET_Seasonal_Reg.RData, DeltaSM_Seasonal_Reg.RData, and DeltaSnow_Seasonal_Reg.RData.

6. This script doesn't use much RAM and doesn't take long to run.

7. The final script csvs.r reads in the previous files and turns them into csv files. A header line including units is included. This script doesn't use much RAM and doesn't take long to run.

Final output

If you successfully follow the preceding steps you should end up with 14 csv files; seven for annual results, and seven for seasonal results. There are seven variables: Ocean (flow to the ocean), Out (flow out of a region into another region), In (flow into a region from other regions), P (precipitation), AET (evaporation), DeltaSM (change in soil moisture), and DeltaSnow (change in snow).

In each csv file you will have a row, named appropriately, for each of the 16regions. Within each row are the values, one per year, or four per year if it is a seasonal file.

Appendix C Evaluating long and short-term ice changes across New Zealand

Aotearoa New Zealand has a relatively short instrument-based weather and climate observational record that extends back into the 1830s (Lorrey and Chappell 2016). Documentation of glacier changes in New Zealand has a similar limitation, and the historic record of ice change only exists from the mid-1800s to present. Primary ice volume and ice areal extent changes that can be demonstrated for the 1800s into the early 1900s come from paintings, sketches and early photography (Figure C-1). While that evidence is sparse, it unequivocally indicates more ice coverage and ice volume used to exist than does today.

Figure C-1: An example of change for a formerly more extensive ice in the Southern Alps shown at Lyell Glacier (upper Rakaia catchment). Left: A view toward Lyell Glacier across Lyell Lake from Meins Knob [photo credit here], which has developed from the recession of a formerly larger Lyell Glacier that used to occupy the valley. Right: Early documentation of Lyell Glacier ice from Meins knob painted by Julius von Haast in the 1860s. The comparison of the modern photograph with the watercolour painting shows the ice occupied a larger volume in the upper Rakaia catchment only 150 years ago, with the upper glacier surface situated close to the trimlines (demarcation between scree and vegetation on the valley sidewalls) observed on both sides of the valley.

Moraines are ridges of poorly sorted sediment that were deposited at the ice-contact margins of formerly larger glaciers. These types of landforms are widely dispersed across the Southern Alps in the foreland regions of glaciers that still exist today. They directly show how ice volume has greatly changed since the end of the Last Glacial Maximum (which ended about 18,000 years ago) when climatic conditions were much colder (Strand et al. 2019). Moraines are useful for determining pre-historic glacier length changes and for confirming historic glacier length change. From the earliest historic records that document the position of ice adjacent to moraines on the west coast at Franz Josef Glacier (Figure C-2) and Fox Glacier (Figure C-3), there has been long-term ice recession through the 20th century with punctuated episodes of ice terminus advance (Purdie et al. 2014).

Geomorphic interpretations of mapped moraines in the central Southern Alps combined with high-precision cosmogenic radionuclide chronologies (generated from surface exposure dating or SED) of Holocene age are now coming online rapidly for New Zealand. The methods that are used to combine mapped glacial landform interpretations with SED results and modelling also provide a holistic way to evaluate pre-historic glacial evidence, with a specific focus linking the timing of ice changes and climatic conditions. For both Mueller Glacier and Cameron Glacier (Figure C-4), about half of their total glacier length (~6.5 and ~2.5 km, respectively) has been lost since the Little Ice Age (LIA; ~1450-1850CE), which corresponds to an associated rise in summer temperatures and a change in regional atmospheric circulation (reduction of trough regimes and an increase in blocking regimes;

Lorrey et al. 2014). Notably, both glacier termini are debris covered at present. Each has broken into separate constituent parts relative to what were formerly larger, coalesced glaciers, and they are both significantly lower in profile at the position of their former LIA halfway point than what they would have been during that time.

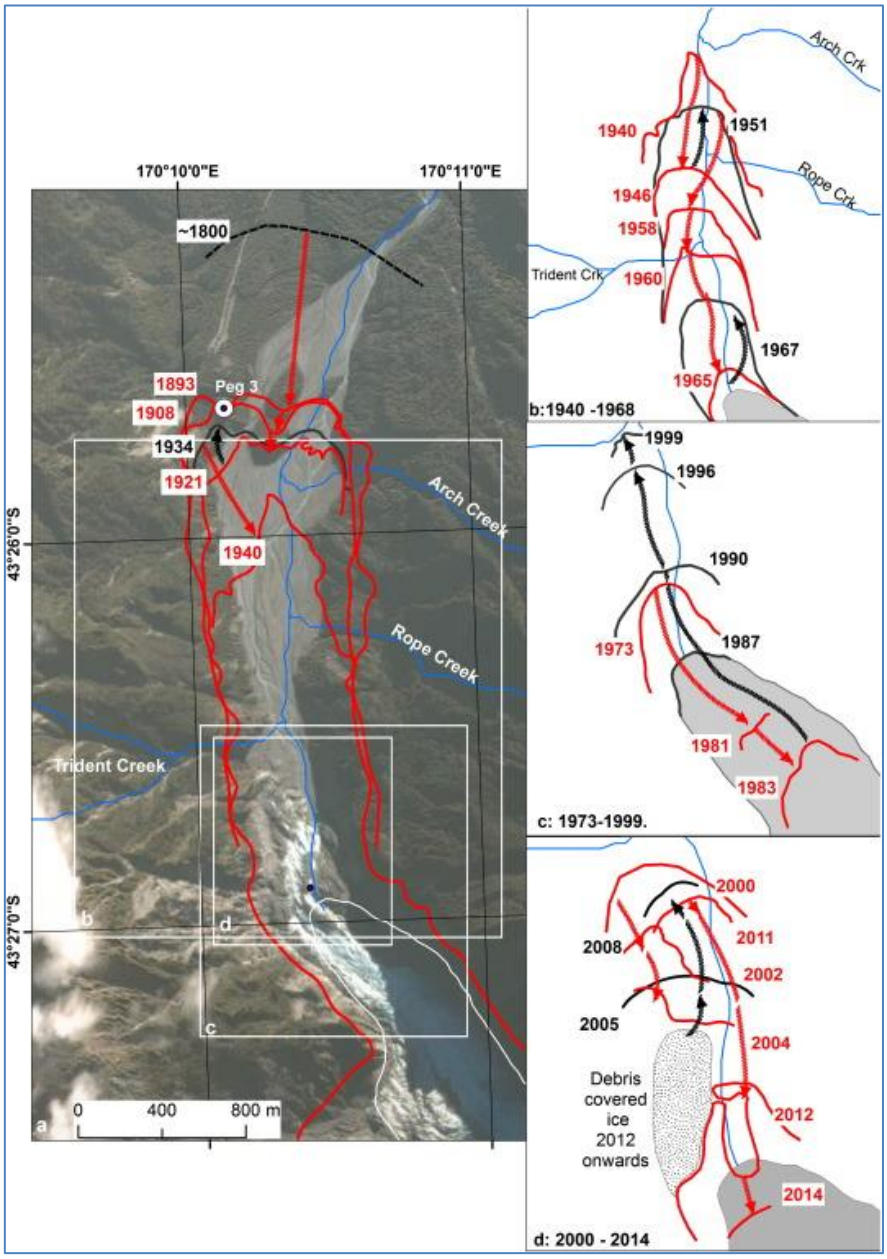

Figure C-2: Franz Josef glacier ice long-term recession and episodic glacier re-advances based on historic mapping covering the late 19th and 20th century. (from Purdie et al. 2014). A.) Debris cover, terminus and fluvial foreland area containing historic recessional moraines of the Franz Josef Glacier. White areas circumscribed cover areas shown on the righthand side that show annual ice margin evidence for 1940-1968, 1973-1999, and 2000-2014. B.) Ice margin positions during1940-1968 show two short re-advances occurred between 1946-1951 (340m) and 1965-1967 (400m) within a period of recession, C.) 1973-1999 shows an initial ice recession (1973-1983), followed by prolonged period of re-advance between 1983-1999 (1420m, almost double the retreat length of the 1973-1983 advance), D.) limited re-advance phases between 2004-2008 (290m) within a period of mostly recession.

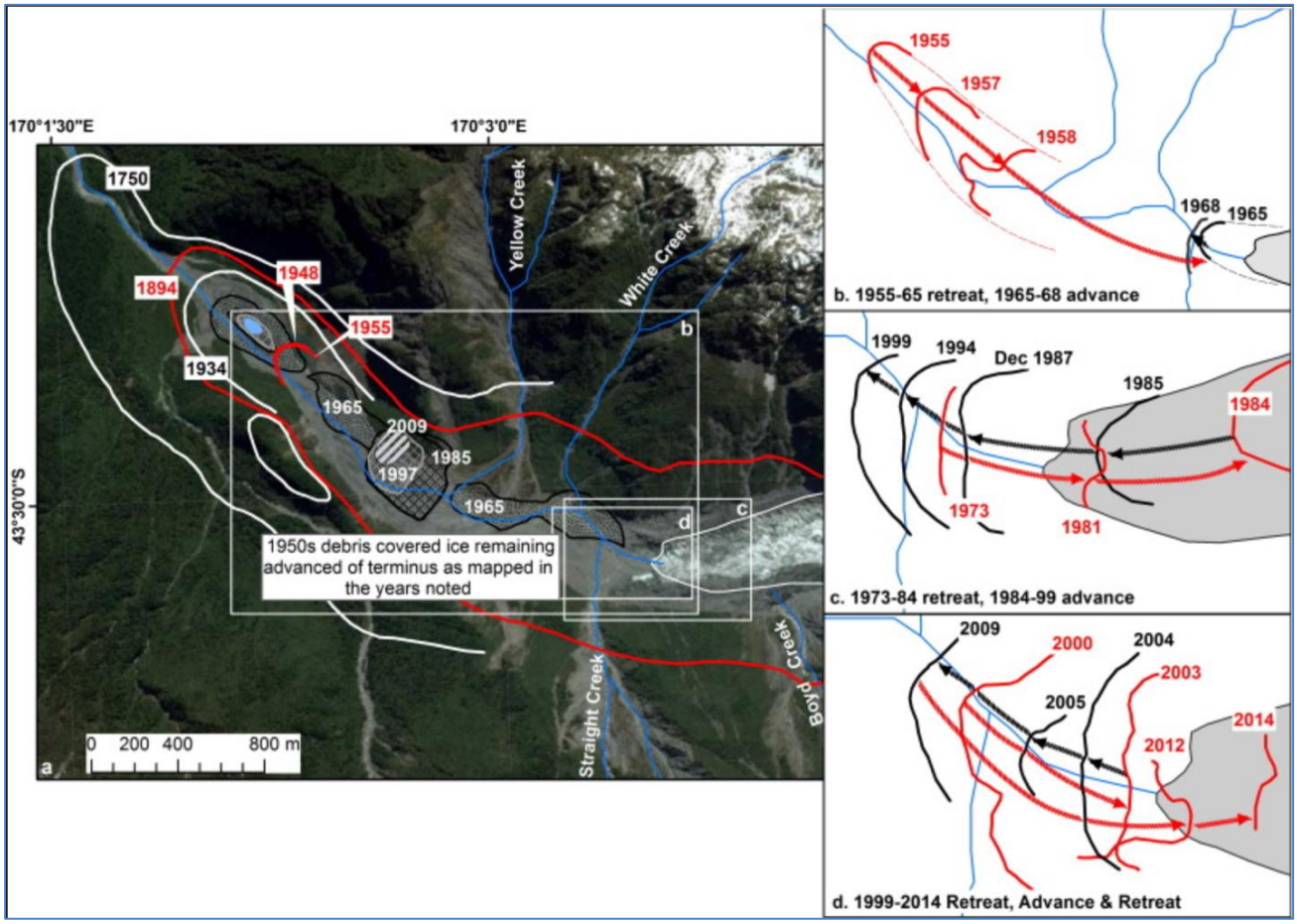

Figure C-3: Fox glacier ice long-term recession and episodic glacier re-advances based on historic mapping covering the late 19th and 20th century. (from Purdie et al. 2014)). A.) Debris cover, terminus and fluvial foreland area containing pre-instrumental and historic recessional moraines of the Fox Glacier. 1750CE ice margin is estimated by landforms constrained by tree-ring dating. White square areas provide more detail (right), and show annual ice margin evidence for 1955-1968, 1973-1999, and 2000-2014, B.) Ice margin positions during1955-1968 show short re-advances occurred between 1964-1968 (60m) at the tail end of a decade largely characterized by ice recession, C.) 1973-1999 shows an initial ice recession (1973-1984), followed by prolonged period of re-advance between 1985-1999 (710 m), D.) There was limited glacier re-advance between 2004-2008 (290m) nested within a period of mostly ice recession.

Mass balance change from in situ monitoring of glaciers

The historic record of monitoring glaciers in situ using a combination of methods is sporadic and limited to fewer than 10 glaciers (most located on the South Island). In situ observations of ice mass balance changes, which is one type of physical change that can be tracked, typically rely on seasonal snow stake measurements which are expensive and time consuming to undertake each year. It is also not practical to undertake ground-based snow stake and mass balance measurements for glaciers spread across an area as large as the Southern Alps. Nevertheless, monitoring for several glaciers is a useful check on remotely sensed observations. NIWA currently supports in situ mass balance survey work at Brewster Glacier and Rolleston Glacier (Figure C-5). NIWA has also restarted observations for Mt Ruapehu, which is expected to become nearly ice-free in the 21st century.

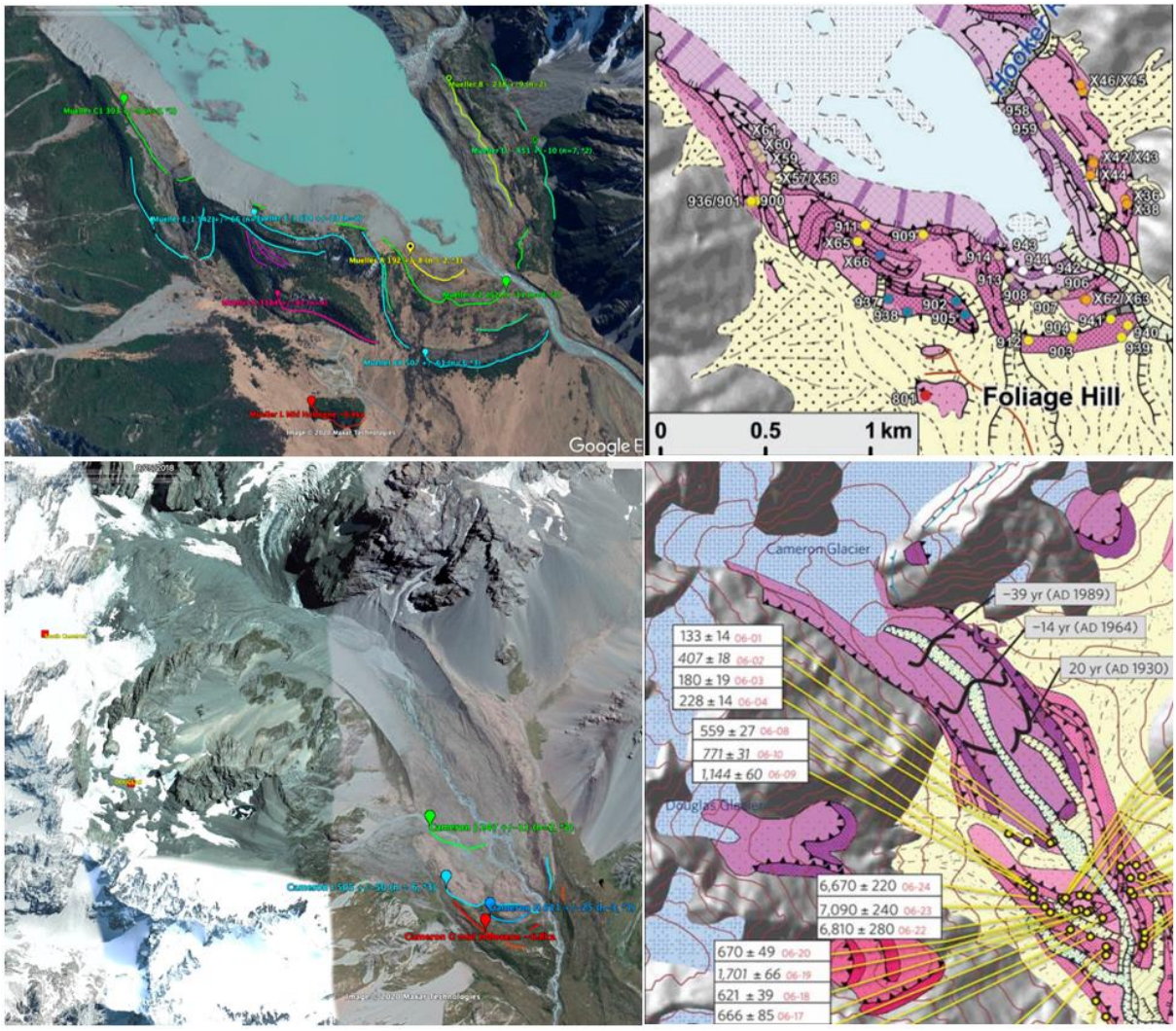

Figure C-4: Recessional moraine sequences within the last 7000 years . with replicated cosmogenic radionuclide dates at Mueller Glacier and Cameron Glacier in the central Southern Alps. (Top left) Aerial imagery shows "bathtub" moraines around Mueller Lake near the Hermitage at Mt Cook, while the geomorphic map (top right, from Schaefer et al. 2006) shows the locations of samples that were dated using SED. (lower left) Aerial image of the convergence of South Cameron, Cameron, and Douglas Glaciers in the Arrowsmith Range, showing the moraine sequence that marks a formerly larger glacier, while the geomorphic map (lower right, from Putnam et al. 2013) shows locations of samples (and ages before 1950CE) that were dated using SED.

.

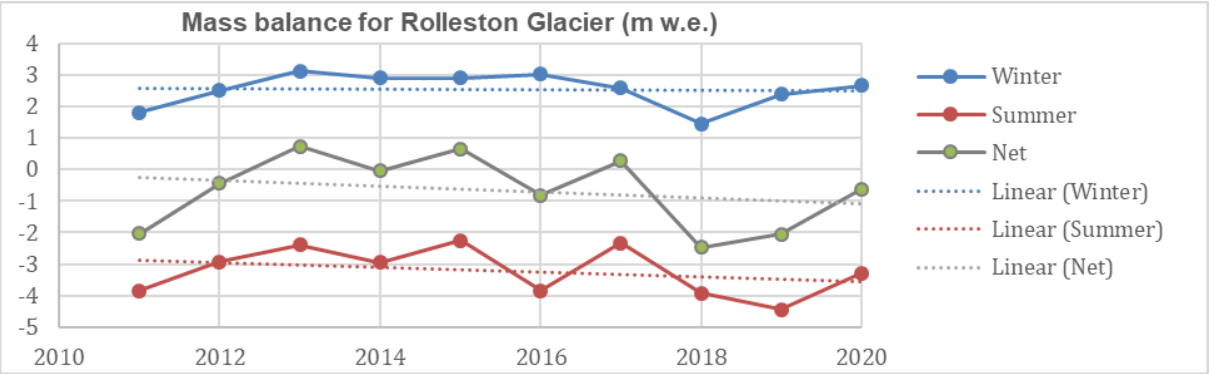

Figure C-5: Interannual mass balance change measured at Rolleston Glacier. The time series results show positive mass balance dominates the winter season when snow falls while negative mass balance typifies the summer months when melt is high. The relatively poor winter mass balance season in 2018 was followed by a poor summer 2018 season made that year one of the worst overall mass balance years for this glacier and others across the Southern Alps.

The observed pattern of cumulative mass balance change, which aggregates both winter and summer mass balance impacts, is replicated between Rolleston Glacier (located in north Canterbury, Arthur's Pass) and Brewster Glacier (located in Mt Aspiring National Park) (Figure C-6). The overall trend since 2010 has seen both glaciers experience a decline in mass balance through the 2019 glacier year (ending March 2019). Rolleston recorded a -6.2 m water equivalent loss and Brewster recorded -5.6 m water equivalent loss during this time. The trend for both seasonal mass balance components suggests a shift toward reduced winter snowfall and warmer summer temperatures (now averaging about -0.5 m water equivalent per year in each of the main winter/summer seasons), which have had dually significant impacts on the net mass balance (now about -1 m water equivalent per annum, achieved by the end of the most recent observational decade).

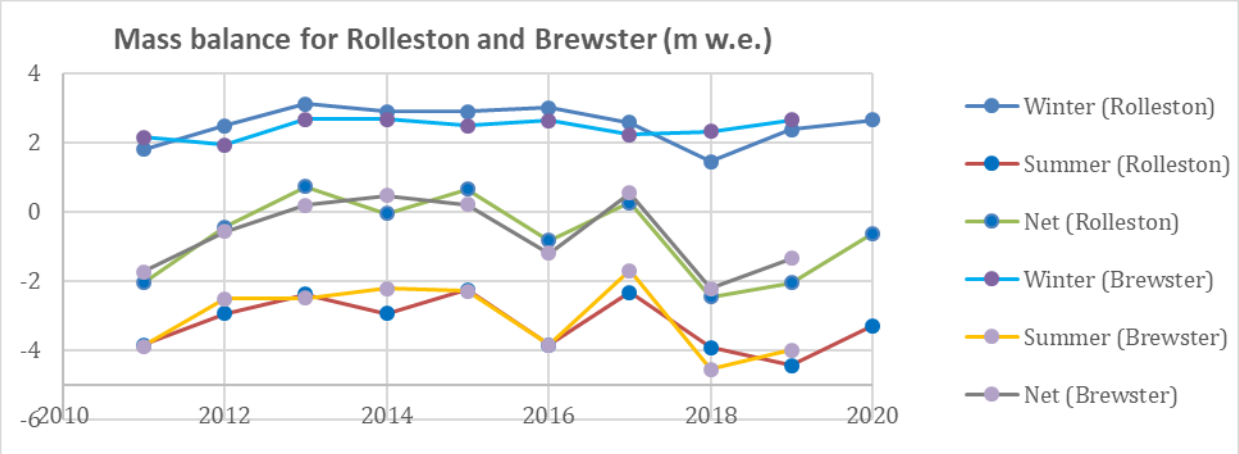

Figure C-6: Mass balance (winter, summer, net) measurements since 2010 from Rolleston and Brewster glacier . using in situ monitoring undertaken by University of Canterbury, University of Otago and Victoria University Wellington. Winter measurement for Brewster glacier to be updated; summer survey not available due to COVID-19 lockdown.

The negative winter mass balance trend for Rolleston since 2010 exists from the inclusion of a much lower than normal snowfall at that site in 2018; but the overall parallel trend toward reduced net mass balance for both Brewster and Rolleston appear similar. The trends are also of similar relative scale when the absolute water equivalent volume amounts are normalised to the 2011-2019 span.

This demonstrates the value of studying multiple glaciers and gathering both the winter and the summer mass balance measurements.

If we also assume that small glaciers like Brewster and Rolleston are dynamic and re-equilibrate to their local climate conditions at the end of each glacier mass balance year, then the inter-annual mass balance change can help to identify common years that were "felt" as largely an improvement or deterioration from the previous year. Positive normalised interannual mass balance change values typically are expressed most strongly after large negative years and vice versa for negative normalised values (Figure C-7). For the most recent decade, it is clear that the interannual variability of climate has been strong, and that the positive interannual mass balance change value for 2017 (when snowlines were observed to be at lower than normal altitudes) stands out against a trend of only moderately variable interannual change. In 2018 when snowlines rose to exceptionally high altitudes, the impact on the interannual mass balance change was prominent (i.e., it was a "shock" year) and also shows that 2019 wasn't much better than 2018.

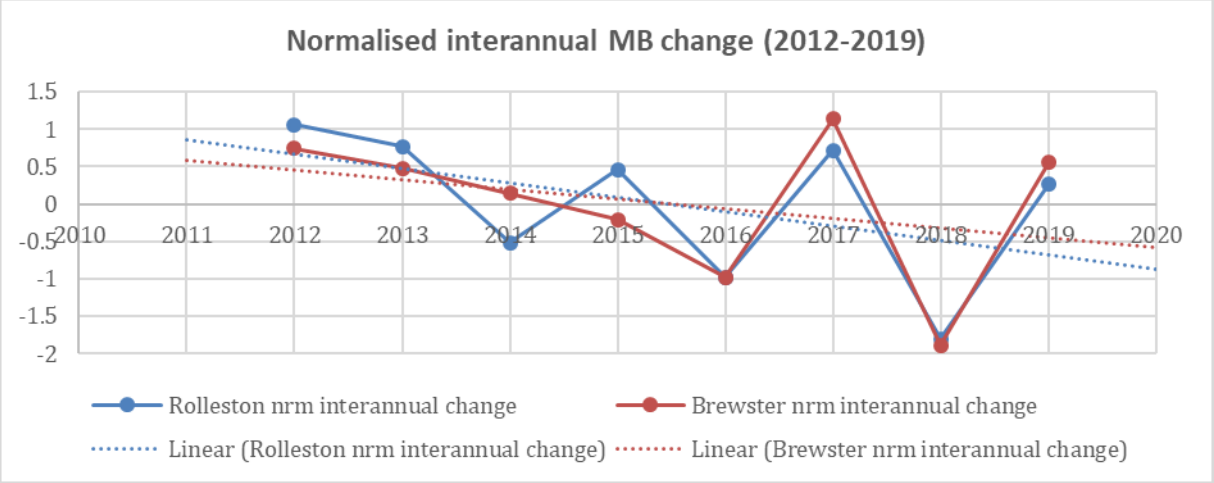

Figure C-7: Normalised interannual mass balance change 2012-2019.

The normalised interannual mass balance change records for Brewster and Rolleston Glaciers indicate how each glacier year compared to the previous year. 2012 was much better than 2011; 2013 was only slightly better than 2012; 2014 was about the same as 2013; 2015 was the same or slightly better than 2014; 2016 was worse than 2015; 2017 was much better than 2016; 2018 was dramatically worse than 2017; 2019 only slightly better than 2018. There is a trend toward each of these glaciers having experienced a worse year than the previous one.

Ice changes estimated from long-term oblique aerial photos

Since 1978, oblique aerial photography has been used on a near-annual basis to capture Southern Alps ice changes by monitoring key index glaciers spread across the Southern Alps (Figure C-8). The index glacier dataset formerly extended from southern Fiordland to Kaikoura, but in recent years it has been increasingly restricted to central Fiordland to north Canterbury due to ice loss at lower altitudes. The index glaciers were originally used to evaluate the end of summer snowline altitude (which is preserved best overlying ice rather than bedrock). These glaciers also represent a range of different sizes and classes of ice masses, from very small glaciers contained in single catchments that have acute-response times to climate (e.g., Rolleston Glacier) to large glaciers that have array of tributaries that terminate in lakes under a debris carapace (e.g., Tasman Glacier). The areal extent, snowline and terminal position of the index glaciers are relatively well-documented (with most index

glaciers having 80% or greater photographic coverage each year since 1978). Since about 2003, NIWA has been responsible for capturing the index glacier observations via the End of Summer Snowline (EOSS) survey that takes place every March.

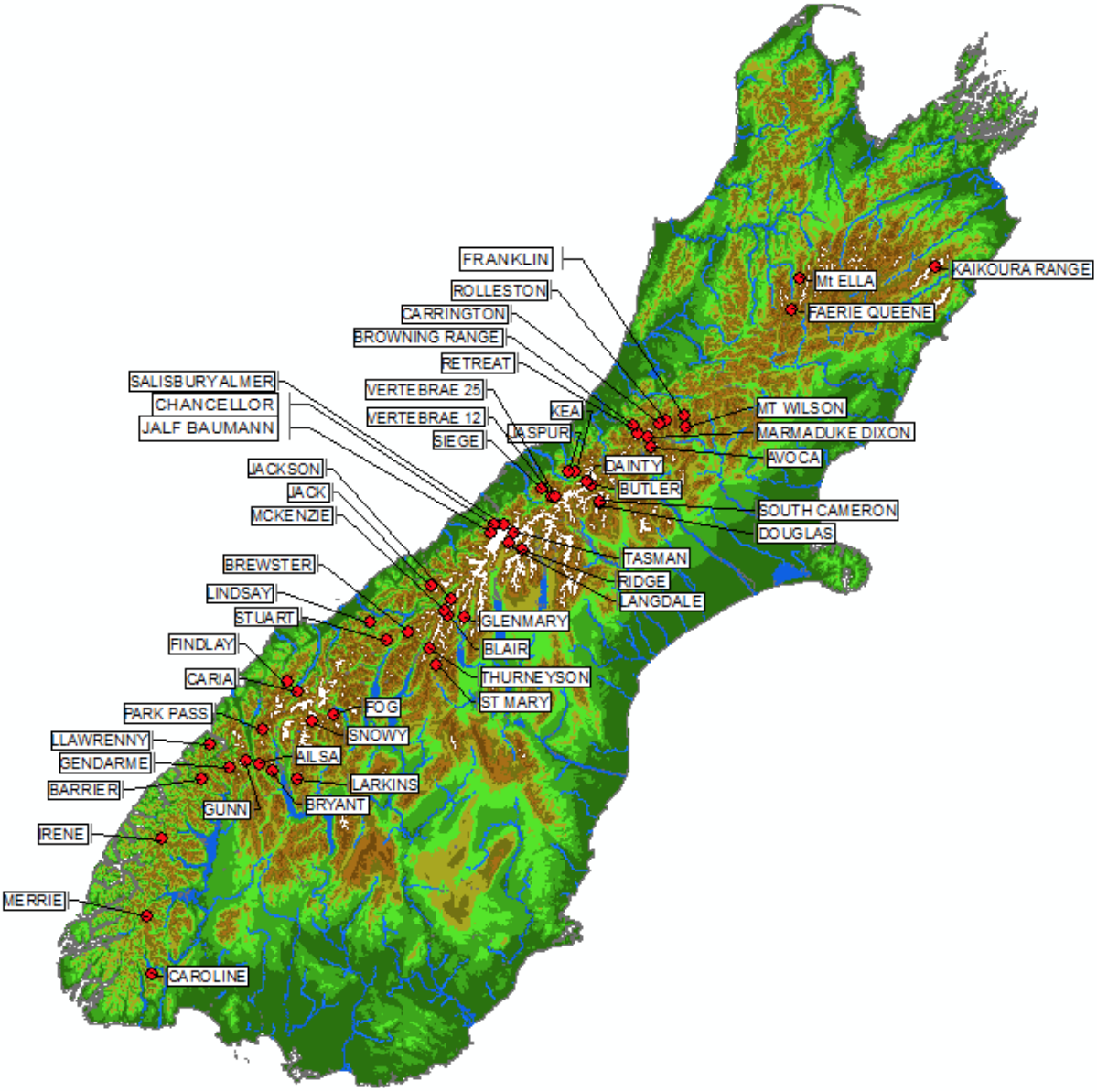

Figure C-8: Locations of South Island New Zealand index glaciers surveyed across the Southern Alps as established by T. Chinn in 1978.

In recent years, the three southernmost sites (Caroline, Merrie, Irene) and the three northernmost sites (Kaikoura Ranges, Mt Ella, and Faerie Queene) have been abandoned. Index glaciers with historic traditional mass balance measurements are maintained on Brewster Glacier and Rolleston Glacier.

Glaciers accumulate net annual mass balance variations spanning individual years to decades. The effects of yearly climate variability can also be delayed and distorted in some situations, depending on the size of the glacier being examined, before they are expressed as a change at the terminal margin of the ice. The EOSS index glaciers appear to record the annual glacier hydrological year climate conditions that influence mass gains and losses with high fidelity, as the majority of them are

small and steep with relatively fast response times. Most of the index glaciers appear to be in equilibrium with the climate of recent years.

Based on pre-processed end-of-summer-snowline (EOSS) data, Willsman (2017) applied a year-specific regression equation that explains the observed volume-area change data for 49 index glaciers (and only where robust observations exist). At present, we understand there are significant errors associated with the absolute values derived using that technique and how it can be improved (Anderson and Mackintosh 2017). Nevertheless, the record of change using the EOSS data is useful for independently evaluating wider changes for snow and ice across the Southern Alps.

Based on the findings of Willsman (2017), ice volume reached a recent temporal maximum of 56.21 km^3 in 1997 relative to an initial volume estimate of 54.02 km^3 in 1977 (an increase of four percent). Volumes then generally declined from 1998, with only a slight rise between 2002 and 2005, followed by near continuous ice volume decline to 2016. By 2016 the total ice volume was estimated a 40.72 km^3. This represented a total loss of 13.29 km^3 (a 24% decrease) from the 1977 starting volume at an average rate of -0.34 km^3a^{-1}.

Twelve large low-angle debris-covered glaciers in the Southern Alps were assumed to not be in instantaneous equilibrium with the current climate (i.e., they are likely still responding to changes that also occurred in the recent and distant past). They are large valley glaciers that have large surface areas that were formerly expanded in a different base climate state (e.g., the LIA and parts of the 20th century). All of them are in a current state of on-going recession, mainly by down-wasting of their debris-covered trunks. Recently, ice loss has accelerated for these glaciers due to the formation of pro-glacial lakes, which enhances tabular calving of ice at terminal margins. This subset of glaciers lost 7.70 km^3 of ice due to proglacial lake growth and trunk down-wasting (a consequence of climate and internal ice dynamics). Therefore, the remaining 5.59 km^3 of ice loss from 1977-2019 calculated by Willsman (2017) can be directly attributed to climatic change.

Cumulative "mass balance indices" (MBIs) are two indices that are based on EOSS data. The cumulative MBI represents the mean departure of the snowline from steady state (ELAo). Snowline departure changes with negative ELA (i.e., lower altitude snowlines) correspond to a positive MBI, and conversely positive ELA departures (i.e., higher altitude snowlines) result in a negative MBI. The reliability of the ELA as mass balance change proxy was investigated by Chinn et al. (2005), where the correlation between the ELA and measured mass balance was significantly positive (average r=0.9 +/- 0.07). Thus, the MBI is an independent but indicative metric of glacier mass balance based on direct snowline altitude estimates from oblique photography (Figure C-9).

The raw cumulative MBI does not agree with the obvious ice volume decrease observed for most of the index glaciers. Over the course of the EOSS monitoring programme, there has been permanent ice loss during large negative mass balance years that has not been recovered after a cycle of positive mass balance years. A negative mass balance year also appears to have a greater impact on ice volume loss than a positive mass balance year does for ice volume gain for MBIs of the same magnitude. This is due to ablation rates typically being almost twice the accumulation rates on most glaciers.

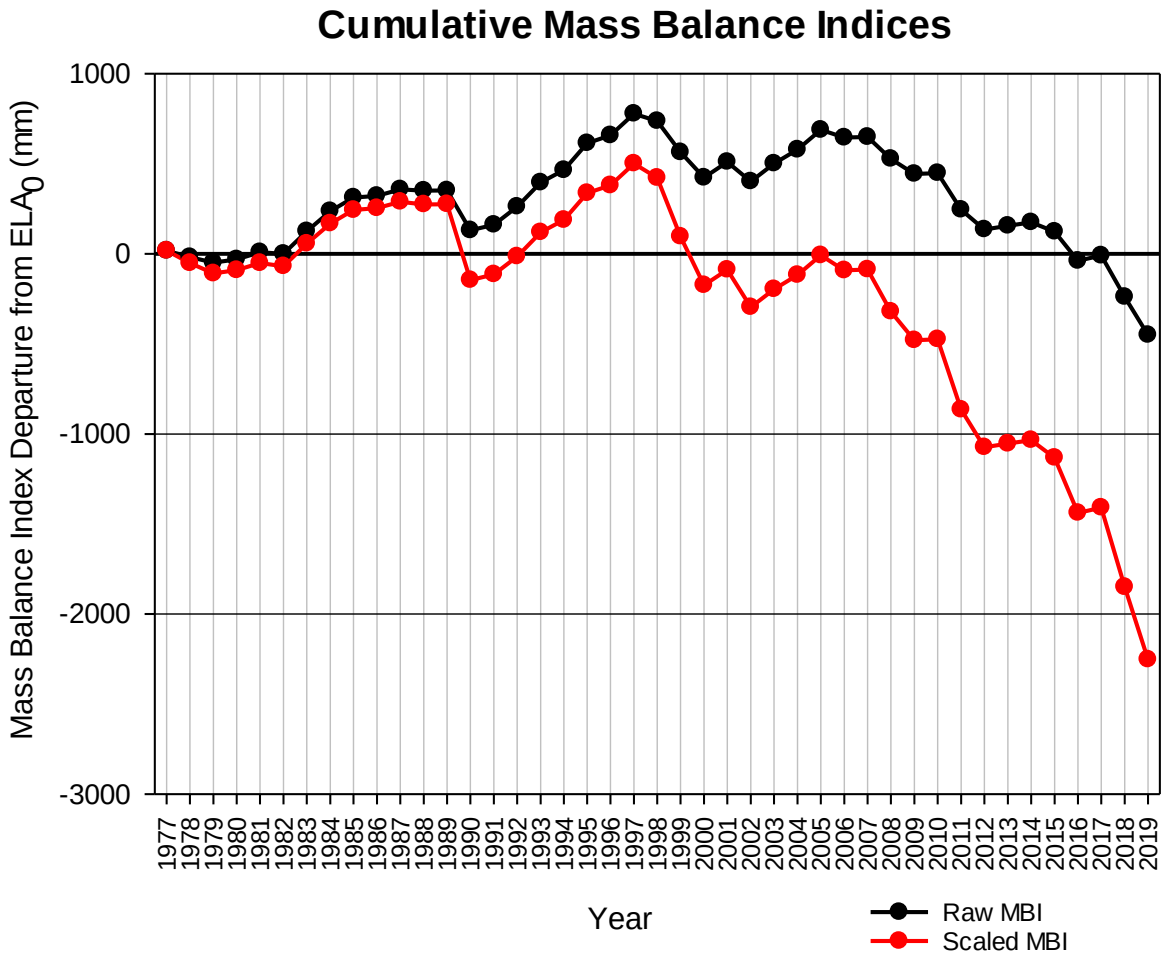

Figure C-9: Raw and Scaled Cumulative Mass Balance Indices for the EOSS index Glaciers following the method of Willsman (2017). Note, both MBI values are dependent on the available index glacier measurements in any given year and are not adjusted further for sample depth changes.

To account for this difference a *scaled mass balance index* is also shown, where negative mass balance years have been multiplied by a factor of 1.92 and a positive mass-balance-year departure, multiplied by 1.0 (i.e., left unchanged). The scaling factors are averages of published mass balance gradient rates from studies on the Tasman (Anderton 1975) and Ivory Glaciers (Anderton and Chinn 1978) for the period 1966-1975. The assumption with this scaling is that the averaged mass balance gradients from previous work apply to the average annual departure values for all of the index glaciers (which may not be correct).

The scaled cumulative MBI shows negative and positive departures from the start of the survey to 2005, when it returns to a position of zero. From 2006 to 2019 the MBI shows a negative trend with short fluctuations of one to two years with near-zero change. The trend in permanent ice area in many of the index glaciers agrees with the cumulative scaled MBI rather than the cumulative raw MBI (which does not account for the mass balance gradient). Further work clearly needs to be done to determine what scaling scheme is appropriate for the index glaciers.

Remote sensing

In recent decades, frequent observations of New Zealand ice have greatly expanded. The first official glacier inventory of New Zealand was undertaken using geodetic maps verified with aerial photos in the late 1970s for the purpose of evaluating the New Zealand hydrological resource held in frozen ice (Chinn 1996, 2001). Glacier outlines for 1978 covering the Southern Alps were initially mapped by hand, with the total number of unique glaciers (~3150) and areal extent and volume of ice (~53 km^3) calculated. The digitized format of the maps comprising the 1978 inventory can be accessed in a GIS from files held in the Randolph Glacier Inventory (RGI), which is an international database available for research. Our recent re-evaluation and understanding of the RGI historic outlines demonstrate that they are not perfect, but errors will be corrected in coming years and are expected to be within 2% of what has been previously catalogued. Nevertheless, the 1978 New Zealand glacier inventory forms a baseline that allows us to evaluate changes that occurred from the 1800s to the late 20th century, and also more recent changes that are now captured annually.

Baumann et al. (2020) recently completed a re-evaluation of the New Zealand glacier inventory using satellite imagery using Landsat 8 using a semi-automatic classification method that defined clean glacier ice which was checked against Sentinel-2 MSI data. They found New Zealand glaciers now cover an area of 794 ± 34 km^2 (as of 2016) with 10% of that area is debris-covered. There were 2918 unique glaciers as of 2016, a reduction of 226 unique ice masses (7.2% of the initial population of 3144 in 1978), although some larger glaciers are likely to have broken into several smaller glaciers. Seven glaciers as of 2016 covered >10 km^2 while 71% of the 2016 population cover <0.1 km^2. The debris cover on the largest glaciers is >40%. Only 15 glaciers are located on the North Island, and cover ~3km^2. Most of our glaciers (92% of the total number) cover only 25% of the total glacierized area of New Zealand. Tasman Glacier remains New Zealand's largest glacier and was 82.8km2 in 2016. The proglacial lake it calves into at the time of evaluation was 6.9km^2. 60% of the total glacierized area of New Zealand lies between 1800 m and 2200 m above sea level.

For a selection of glaciers, Baumann et al. (2020) calculated the area reduction between the 1978 and 2016 New Zealand glacier inventories. Tasman Glacier reduced from 101.6 km^2 to 82.8 km^2 (loss of 18.7% areal coverage from 1978), while Murchison Glacier reduced by 28% during the same time (33.9 km^2 to 24.4 km^2). Overall the largest 14 glaciers surveyed for New Zealand experienced an average areal reduction of ~21%, and without including Fox and Franz Josef, that figure expands to ~27% areal reduction (Figure C-10).

Recent work has extended the understanding of New Zealand glacier geometry between the Little Ice Age (LIA) and the late 20th century. The LIA is defined as ~1450-1850CE in New Zealand based on quantitative tree ring temperature reconstructions that indicate summer temperatures were ~0.5C lower than modern times (Lorrey et al. 2008, 2014) The ice changes defined for the LIA to the late 20th century have focused on ice areal extent and ice volume estimations. As with other techniques used to evaluate ice changes, there are multiple methods employed and each has certain advantages and idiosyncratic uncertainties when applied across the Southern Alps.

A new method for outlining LIA glacier extent across the Southern Alps has relied on the RGI outlines (see comments above) and is described in Carrivick et al. (2020). In that study, they used a hillshade 8 m digital elevation model (DEM) and a further 1m optical image resolution that targeted sharp-crested moraine and associated trim lines in the foreland regions of modern New Zealand glaciers that have recently receded. The innermost moraine for LIA sequences that have multiple landforms were used to obtain a conservative estimate of the ice margin position at the end of the LIA. In addition, an ice-free DEM was derived by subtracting estimates of modern ice thickness from a base

DEM using methods defined in Carrivick et al. (2020). A discussion of the changes from 1978-Present was included by Carrivick et al. (2020), but has been superseded by Baumann et al. (2020) (see previous section for details).

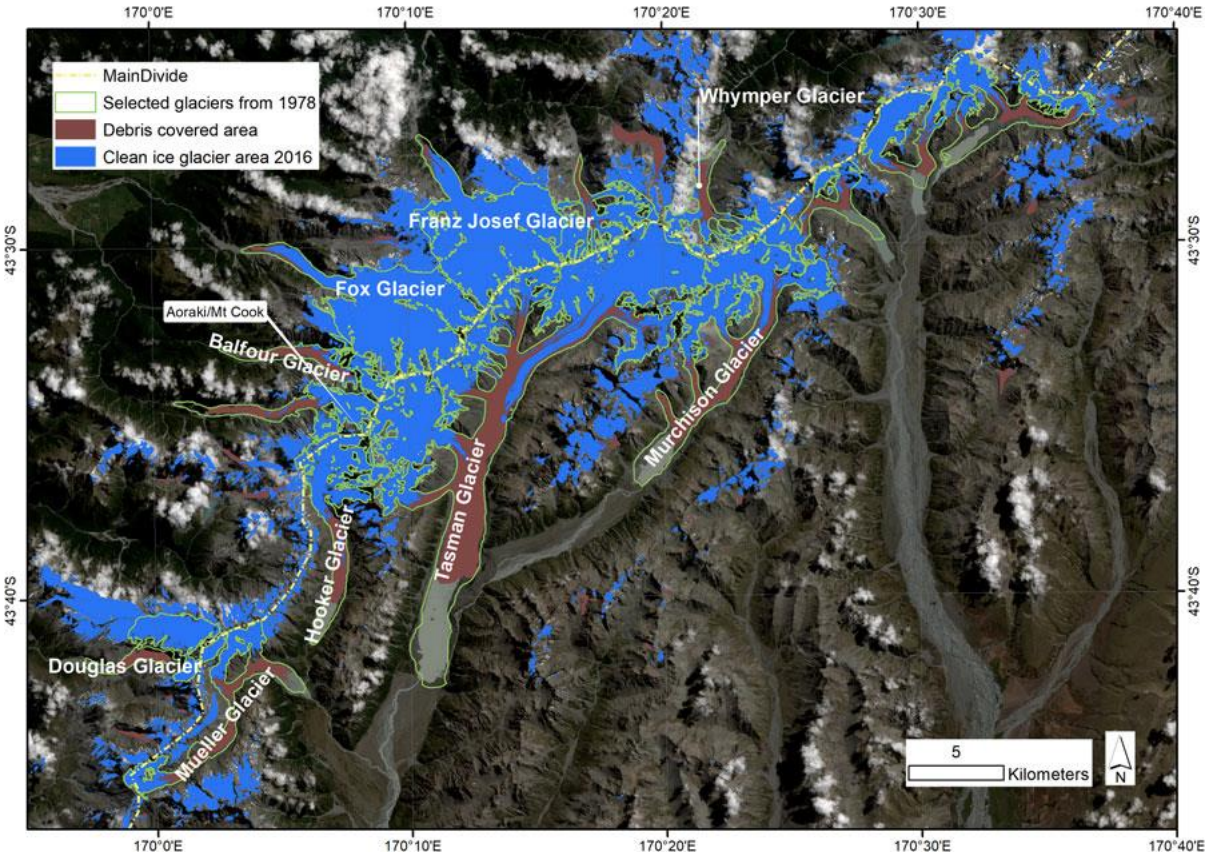

Figure C-10: Central Southern Alps with a focus on Mt Cook region. showing many "long-response" glaciers that have debris-covered carapaces in the ablation zone that terminate in proglacial lakes. Green is the outline of glacier extent in 1978, blue is clean ice area in 2016, brown is debris-covered glacier ice in 2016. Mapping was undertaken using Sentinel-2 MSI from 12 February 2016 (after Baumann et al. 2020).

Carrivick et al. (2020) estimated 1492 km^2 +/104 km^2 of ice coverage that formerly existed during the LIA is now gone. In addition to glacierized area covering 440 km^2 that is above modern ice coverage (which could not be mapped), that study suggests at least 1932 km^2 +/- 135 km^2 of total ice coverage existed during the LIA across the Southern Alps. RGI coverage shows an area coverage of 1463 km^2 (no errors estimated) in 1978 (based on Chinn's methods). When the LIA findings are evaluated relative to that survey datum, it is estimated that 334-604 km^2 reduction in glacierized area occurred from the LIA to late 1970s. That change equates to 19-29% areal coverage reduction of what was formerly glaciated landscape during the LIA. A very small percentage (~10%) of land that is presently glacierized lies within the formerly larger ablation zone where larger LIA glaciers once existed. This reflects the long-term change in the snowline (equilibrium line) altitude rising in response to rising temperatures from the late 19th century to the late 20th century.

Changes in interannual ice volume in recent years – an example using Brewster Glacier geodetic mass balance change from high-resolution DEMs

A relatively novel approach has been recently applied to the Southern Alps to quantify glacier volume change from EOSS photos of the index glaciers. The method involves using aerial photographs with Structure-from-Motion Photogrammetry (SfM) software to generate 3-D models of the glaciers (Vargo et al. 2017). From the 3-D models, annual digital elevation models (DEMs) of the glaciers are created. By comparing these DEMs between different years the change in ice volume, also known as geodetic mass balance, can be calculated.

The DEM generated from March 2016, along with three different DEMs generated in 2019 (generated using different methods of georeferencing), have been analysed. Using the three different 2019 DEMs allows testing of the accuracy of the method and calculated uncertainties. All DEMs are georeferenced using images from a previous year, with all snow and ice masked, in order to match the bedrock in 2019 images with bedrock in SfM models that are already georeferenced.

Using the DEM with the lowest root mean square error (Table C-1; test a), we find a geodetic mass balance of -6.84 ± 1.34 meters of water equivalent (m w.e.). Using the same DEM georeferenced only slightly differently, using all 10 ground control points (GCPs) instead of five (Table C-1; test b), we find a similar mass balance of -6.80 ± 1.34 w.e. The identical uncertainties between test a and test b are representative of the small change in georeferencing. Finally, in test c we use a DEM georeferenced using a 2016 SfM model (Table C-1). The calculated mass balance of -6.44 m w.e. still falls within the uncertainties of the other two tests, with a similar but slightly lower uncertainty of ± 1.23 m w.e.

Table C-1: The three different 2019 DEMs used, and resulting calculated geodetic mass balance from March 2016 - March 2019.

Test	Brewster 2019 dem	Dem Georeferencing method	Geodetic mass balance (m w.e.)
a	brewster_2019_dem_clip.tif	Using 2017 DEM, using ½ of GCPs to georeference and ofthe ½ to calculate RMSE	-6.84 ± 1.34 m w.e.
b	2019_dem_t2_clip.tif	Masked using 2017 DEM, and all GCPs	-6.80 ± 1.34 m w.e.
c	2019_dem_2016mask_clip.tif	Masked using 2016 DEM	-6.44 ± 1.23 m w.e.

There is a large difference between the geodetic mass balance and measured glaciological mass balance for Brewster Glacier from March 2016 through March 2019. The glaciological mass balance from is -3.00 m w.e., with an uncertainty of ~0.3 m w.e. (Sirguey 2019), compared to the geodetic measurements of -6.84 ± 1.34 m w.e. (Table C-1). Possible reasons for the discrepancy include:

1. That glaciological mass balance measurements are made only on the lower glacier below ~2000 m a.s.l., as the upper glacier (~2000 - 2400 m a.s.l.) is steeper and less safe to access with possible avalanche hazards.

2. Biases in glaciological measurements. Glaciological measurements assume that no melt occurs between when the summer measurement is made, and winter measurement is made. However, the summer measurements were made between 15

and 23 March, while mass balance modelling using a degree-day model suggest that melt can occur through mid to late April. This discrepancy should always bias glaciological measurements to be more positive than they really are, which is consistent with our findings here. The reason for making summer measurements in mid-March instead of mid-April is safety- from mid-March to mid-April there is usually some new snowfall on the glacier, making it less safe than when there is no new snow.

3. Timing of the glaciological mass balance winter measurements. Winter balance measurements for the years analysed here were made between 10 and 30 November. It is possible that either more snow could have fallen after those dates, or melt occurred before those dates.

Supplementary material on methods

Willsman (2017) derivation of ice volume change from EOSS photos

The methodology used by Willsman (2017) for estimating ice volume change was developed by Trevor Chinn and others in 2007, and subsequently published in 2012 (Chinn et al. 2012). It utilises EOSS measurements from index glaciers 1977-present. Willsman (2017) presented total Glacier Ice Volume for New Zealand, as opposed to regional breakdowns of some earlier reports (e.g., Willsman 2011) due to the difficulty applying model/methodology to very small ice areas/volumes in some regional areas. Ice volumes are representative of glacier years (1 April – 31 March), such that 2016 ice volume value represents the situation as at 31 March 2016, and EOSS used for 2016 calculation represents the elevation of the snowline remaining after the 1 April 2015 – 31 March 2016 year of snow accumulation and melt.

Ice volume change methodology:

- Annual EOSS, Avg EOSS and ***mass balance gradient*** used to calculate annual ice volume change for each index glacier;
- Annual volume change divided by respective index glacier area to derive an annual net balance, these annual net balances averaged to derive an average annual net balance;
- Average annual net balance applied to areas of remaining glaciers (excluding 12 large debris-covered glaciers) to derive an annual volume change;
- Annual volume change applied to ***initial ice volume*** (54.02 km^3) taken from 1978 New Zealand Glacier Inventory (Chinn 2001).

Initial Ice Volume:

- Determined by applying “current methodology” as used in Willsman (2017) to 1978 NZ Glacier Inventory (Chinn 2001).

Mass Balance Gradient:

- Fixed, but relatively low at high elevation, and relatively high at low elevation. This accounts for the difference between relatively low melt rate of snow/firn at high elevations vs. relatively high melt rate of exposed ice (high surface roughness and relatively low albedo) at low elevations. In addition, this accounts for the assumption that the accumulation area of a glacier is twice that of the ablation area.
- Mass balance gradient used in earlier reports (e.g., Willsman 2011) was obtained from 1966-1975 data via the Ivory (Anderton and Chinn 1978) and Tasman (Anderton 1975) Glaciers. Ivory Glacier was deemed representative of glaciers west of the main divide,

with a mass balance gradient of 12.9 mm/m for the accumulation zone, and 25.8 mm/m for the ablation zone (Chinn et al. 2012). Tasman Glacier was chosen as representative of the eastern region, with a mass balance gradient of 7.5 mm/m for the accumulation zone, and 15.0 mm/m for the ablation zone (Chinn et al. 2012).

- Willsman (2017) differs from earlier reports (e.g., Willsman 2011), by applying a longer and more recent mass balance gradient dataset obtained from Brewster Glacier (2000-2015; Cullen et al. 2016).
- As reported in Willsman (2017), original mass balance parameters (i.e., 1965-75 mass balance gradient) considerably overestimated annual net balance compared to that observed at Brewster Glacier, especially during negative balance ice loss years e.g., 2002, 2011 and 2012. The scale of volume change using 1965-75 mass balance gradient is therefore greater than expected. For these reasons, averaged Brewster Glacier mass balance gradient data (2000-2015; Cullen et al. 2016) used for annual net balance inputs to the model in Willsman (2017), i.e., accumulation rate 7.4 mm/m, ablation rate 14.5 mm/m.

A modified methodology (using 2000-2015 Brewster Glacier mass balance gradient; Cullen et al. 2016) results in improved estimation of glacier ice volume change. However, a recent paper by Anderson and Mackintosh (2017) demonstrates that it still overestimates the magnitude of glacier mass balance change. The authors proposed an improved method of applying the mass balance gradient.

- At present, the mass balance gradient is applied such that the 'relatively low rate' is used for elevations above the annual EOSS (as measured on the annual EOSS flights), and the 'relatively high rate' is used for elevations below the annual EOSS (Figure C-11; left), resulting in high annual variability.
- Anderson and Mackintosh (2017) 'fix' the mass balance gradient shift (from low gradient to high gradient) at the glacier's long-term average Equilibrium Line Altitude (ELA); however the 'curve' is offset horizontally so that mass balance = 0 at the annual ELA (i.e., the annual EOSS via the EOSS flights). This is shown in Figure C-11 (right). This reduces the high annual variability of the former Willsman 2017 method, and is thought to better represent the in-situ glacier response.

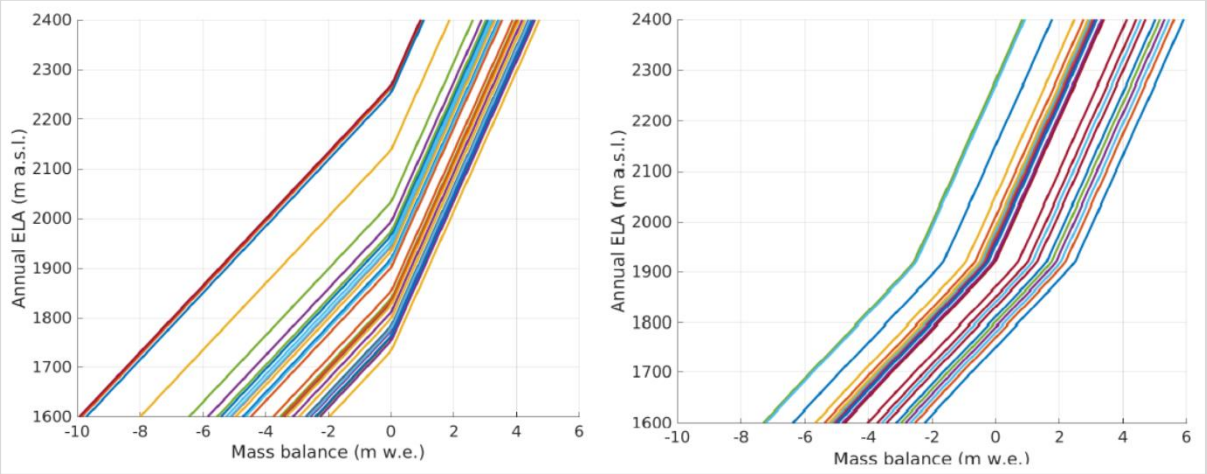

Figure C-11: Methods for applying mass balance gradients. (Left) The method of applying mass balance gradients above and below the annual ELA used by Chinn et al. (2012) and Willsman (2017). (Right) Anderson and Mackintosh (2017) propose an improved method of applying mass balance gradients relative to the long-term ELA, while maintaining the annual ELA at zero mass balance. Each line corresponds to the assumed mass balance vs elevation relationship for an individual year, based on the observed annual ELA. Source: Anderson and Mackintosh (2017).

Brewster Glacier was used to develop and test the SFM method (Vargo et al. 2016). DEMs from Brewster Glacier were compiled from March 2016 and March 2019 to calculate the geodetic mass balance over that same time. In addition to differencing the DEMs to calculate volume change, additional steps to increase the accuracy of the method in Vargo et al. (2016) have been added. They include:

- The SfM DEMs have associated errors of approximately 1 m. We therefore co-register the two DEMs to each other- matching the DEMs to each other based on areas within each DEM that are unchanging (stable bedrock). This co-registration increases the accuracy of ice volume change calculations.
- The SfM DEMs can have pixels or groups of pixels with unreasonable values. This can be due to poor coverage of photos, steep terrain, and/or areas of bright snow that are not always captured well in photographs. To address this issue, once the difference in the outlined glacier in the two DEMs (dH) is calculated, we remove outliers. Any pixels in dH that are greater than ± 5 standard deviations of the mean are removed. This step also increases the accuracy of ice volume change calculations.

Additional steps to calculate the associated uncertainties with calculated volume change have been incorporated based on Zemp et al. (2019). These include:

- Density - we use an ice density of 850 ± 60 kg m^{-3} following Zemp et al. (2019). The two years being compared here, 2016 and 2019, were both years when the glacier was largely snow-free at the time of the snowline flight and photo acquisition. Therefore, the uncertainties from density are smaller than if the glacier had snow cover in one or both years.
- Area - again following Zemp et al. (2019), we initially use an uncertainty for glacier area of ± 5%. Areas are calculated by manually digitizing the glacier outlines on respective annual SfM orthophoto mosaics. Uncertainties arise from the human error, both in

manually digitizing, and in determining what is glacier ice or dead ice (no longer part of the glacier).

- DEM uncertainty - the largest component of the total uncertainties in volume calculations comes from uncertainties in the DEMs used. This is calculated by differencing the DEMs with the glacier masked, to see only the difference in bedrock, which is assumed to be stable. The difference in bedrock pixels from the DEMs results in a normal distribution with a mean of -0.099 m, and standard deviation of 1.43 m. We use that standard deviation from the mean to calculate the uncertainty from the DEMs.

SFM photogrammetry

- The method developed has been scripted, enabling the workflow to be used for future years (needing only to input a new DEM and glacier outline) or for different glaciers. The code is available at https://github.com/lvargo13/geodetic_mb.

References for Appendix C

Anderton, P.W. and Chinn, T.J., (1978) Ivory Glacier, New Zealand, an IHD representative basin study. Journal of glaciology, 20(82), pp.67-84.

Anderson, B. and Mackintosh, A. (2017) Glacier Mass Changes in the Southern Alps 1972-2016. Report to the Ministry for the Environment, 27p.

Anderton, P. W. (1975) Tasman Glacier 1971-73. Hydrological Research. Annual Report No. 33. Ministry of Works and Development for the National Water and Soil Conservation Organisation, Wellington, New Zealand. 28p.

Anderton, P. W. and Chinn, T. J. (1978) Ivory Glacier, New Zealand, an IHD basin study. *Journal of Glaciology*. 20 (82), pp. 67-84.

Baumann, S., Anderson, B., Chinn, T., Mackintosh, A., Collier, C., Lorrey, A.M., Rack, W., Purdie, H. and Eaves, S. (2020) Updated inventory of glacier ice in New Zealand based on 2016 satellite imagery. Journal of Glaciology, pp.1-14.

Carrivick, J. L., James, W. H. M., Grimes, M., Sutherland, J. L. and Lorrey, A. M. (2020) Ice thickness and volume changes across the Southern Alps, New Zealand, from the little ice age to present. *Scientific Reports*. 10: 13392, https://doi.org/10.1038/s41598-020-70276-8

Chinn, T. J. (2001) Distribution of the glacial water resources of New Zealand. *Journal of Hydrology* (NZ) 40(2), pp. 139–187.

Chinn, T. J., Willsman, A., Salinger, M. J. (2005) Glacier Snowline Survey, 2005. *NIWA Client Report* AK:2005-083.

Chinn, T.J., Fitzharris, B. B., Willsman, A., Salinger, M. J. (2012) Annual ice volume changes 1976-2008 for the New Zealand Southern Alps. *Global and Planetary Change*. 92-93, pp. 105-118.

Cullen, N. J., Anderson, B. A., Sirguey, P., Stumm, D., Mackintosh, A., Conway, J. P., Horgan, H. J., Dadic, R., Fitzsimmons, S. J., Lorrey, A. (2016) An 11-year record of mass balance of

Brewster Glacier, New Zealand, determined using a geostatistical approach. *Journal of Glaciology*, pp. 1-19.

Lorrey, A.M. and Chappell, P.R., (2016) The "dirty weather" diaries of Reverend Richard Davis: Insights about early colonial-era meteorology and climate variability for northern New Zealand, 1839-1851. Climate Past, 12, pp.553-573.

Lorrey, A., Fauchereau, N., Stanton, C., Chappell, P., Phipps, S., Mackintosh, A., Renwick, J., Goodwin, I. and Fowler, A., (2014) The Little Ice Age climate of New Zealand reconstructed from Southern Alps cirque glaciers: a synoptic type approach. Climate Dynamics, 42(11-12), pp.3039-3060.

Purdie, H., Anderson, B., Chinn, T., Owens, I., Mackintosh, A. and Lawson, W., (2014) Franz Josef and Fox Glaciers, New Zealand: historic length records. Global and Planetary Change, 121, pp.41-52.

Sirguey, P. Brewster Glacier mass balance (2019) Unpublished report (2019).

Vargo, L. J., Anderson, B. M., Horgan, H. J., Mackintosh, A. N., Lorrey, A. M., & Thornton, M. (2017) Using structure from motion photogrammetry to measure past glacier changes from historic aerial photographs. *Journal of Glaciology*, *63*, 1105-1118.

Willsman, A. (2011) Annual glacier ice volumes in New Zealand 1995-2010. Prepared for Statistics New Zealand, NIWA Client Report CHC2011-050. 19p.

Willsman, A. (2017) Annual glacier ice volumes, 1977-2016. Prepared for Ministry for the Environment, NIWA Client Report 2017127EI. 20p.

Zemp, M., Huss, M., Thibert, E. *et al.* (2019) Global glacier mass changes and their contributions to sea-level rise from 1961 to 2016. *Nature* 568, 382–386. https://doi.org/10.1038/s41586-019-1071-0